
Master's Thesis

APPARATUS TO DELIVER LIGHT TO THE TIP-SAMPLE INTERFACE OF AN
ATOMIC FORCE MICROSCOPE (AFM)

by

Erik Jan Thoreson

A Thesis

Submitted to the Faculty

of the

WORCESTER POLYTECHNIC INSTITUTE

in partial fulfillment of the requirements for the

Degree of Master of Science

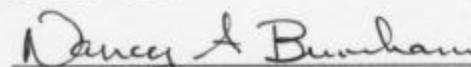
in

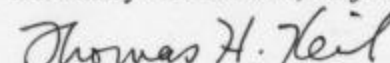
Physics

By


August 2002

APPROVED:


Dr. Nancy A. Burnham, Major Advisor


Dr. Thomas H. Keil, Head of Department

Abstract

An apparatus for the delivery of radiation to the tip-sample interface of an Atomic Force Microscope (AFM) is demonstrated. The Pulsed Light Delivery System (PLDS) was fabricated to probe photoinduced conformational changes of molecules using an AFM. The PLDS is 67 mm long, 59 mm wide, and 21 mm high, leaving clearance to mount the PLDS and a microscope slide coated with a thin film of photoactive molecules beneath the cantilever tip of a stand-alone AFM. The PLDS is coupled into a fiber pigtailed Nd:Yag frequency doubled laser, operating at a wavelength of 532 nm. The radiation delivered to a sample through the PLDS can be configured for continuous or pulsed mode. The maximum continuous wave (CW) power delivered was 0.903 mW and the minimum pulse width was 12.3 μ s (maximal 401 μ s), corresponding to a minimal energy of 0.150 nJ (maximal 362 nJ), and had a cycle duration of 10.0 ms. The PLDS consists of micro-optical components 3.0 mm and smaller in diameter. The optical design was inspired by the three-beam pick-up method used in CD players, which could provide a method to focus the pulse of light onto the sample layer. In addition, the system can be easily modified for different operational parameters (pulse width, wavelength, and power). As proof that the prototype design works, we observed a photoinduced 'bimetallic' bending of the cantilever, as evidenced by observing no photoinduced bending when a reflective-coated cantilever was replaced by an uncoated cantilever. Using the apparatus will allow investigation of many different types of molecules exhibiting photoinduced isomerization.

Acknowledgements

I really appreciate my wife for her undying support and love. Jamie has been instrumental in helping me achieve this step in my life.

My parents for their support and love

Above all, I would like to thank God for my success in life so far. Lord willing, I will continue to be directed by his path for many years to come.

Definitions

a	Smallest diameter spot size
ADP	Adenosine diphosphate
AFM	Atomic Force Microscope
AOM	Acoustic Optical Modulator
ADP	Adenosine diphosphate: organic base with two phosphate groups; combines with another phosphate to make ATP.
ATP	Adenosine triphosphate: Energy stored in ATP is used in most endergonic reactions in cells
BL	Ball Lens
CD	Compact Disk
CW	Continuous Wave
CL	Cylindrical Lens
C	Circularly polarized light
Chemical Energy	Potential energy stored by electrons in a chemical bond
DC	Direct Current
Endergonic Reaction	Reaction that absorbs energy from its surroundings
E_{photon}	Energy of a photon
Enzyme	protein used to catalyze a specific biochemical reaction
FC/APC	Fiber Connector / Angled Physical Contact
FC/PC	Fiber Connector / Physical Contact
F_{number}	Effective focal length of a lens, divided by the diameter
HOMO	Highest Occupied Molecular Orbital

L	Lens
LUMO	Lowest Unoccupied Molecular Orbital
λ	Wavelength of light (532nm)
Metabolites	substance essential to metabolism
NADPH	Nicotinamide Adenine Dinucleotide Phosphate Hydrogen: the reduced form of NADP
NADP	an enzyme that accelerates the removal of hydrogen from metabolites and its transfer to other substances
ND:YAG	Neodymium:Yttrium-Aluminum Garnet
$\frac{N_{ph}}{molecule}$	Number of photons per molecule
nsec	Nanosecond
NSOM	Near-field Scanning Optical Microscope
P	reflecting right angled Prism
PBS	Polarizing Beam Splitter
P _{CW}	Continuous wave power
PDAC	Polydimethyliallammonium Chloride
Photophosphorylation	Synthesis of ATP from ADP and phosphate from photostimulation.
PLDS	Pulsed Light Delivery System
PSPD	four-quadrant Position-Sensitive PhotoDiode
PM	Polarization Maintaining
PW	Primary Wave; transverse electric component of the electric field

w	Pulse width of the input to the AOM
QWP	Quarter Wave Plate
r_m	Radius of Molecule
r_b	Radius of Beam
SW	Secondary Wave; transverse magnetic component of the electric field
WT-bR	Wild-Type Bacteriorhodopsin

Contents

APPARATUS TO DELIVER LIGHT TO THE TIP-SAMPLE INTERFACE OF AN ATOMIC FORCE MICROSCOPE (AFM)

<i>Acknowledgements</i>	<i>ii</i>
<i>Definitions</i>	<i>iii</i>
<i>List of Figures</i>	<i>viii</i>
<i>List of Tables</i>	<i>1-9</i>
1 INTRODUCTION	1-1
2 BACKGROUND.....	2-2
2.1 <i>Paraxial approximation and Snell's law</i>	2-2
2.2 <i>Fiber optics</i>	2-5
2.3 <i>Optics</i>	2-15
2.4 <i>Photoinduced and chemical-induced cantilever deflection</i>	2-16
2.5 <i>Photoinduced molecular conformations</i>	2-20
3 EXPERIMENTAL METHODS AND APPARATUS	3-1
3.1 <i>Apparatus</i>	3-1
3.2 <i>Procedure</i>	3-7
3.3 <i>Sample</i>	3-10
4 RESULTS	4-1
4.1 <i>Power</i>	4-1
4.2 <i>Energy and number of photons delivered</i>	4-2
4.3 <i>Polarization</i>	4-3
4.4 <i>Spot size</i>	4-3

4.5	<i>Alignment</i>	4-4
4.6	<i>Surface roughness</i>	4-5
4.7	<i>Cantilever deflection</i>	4-7
5	DISCUSSION	5-1
5.1	<i>PLDS performance</i>	5-1
5.2	<i>Sample</i>	5-3
6	CONCLUSIONS AND FUTURE WORK	6-1

APPENDIX

A.	DECIBEL	A-1
B.	SKETCHES AND PHOTOGRAPHS	B-1
C.	DESIGN REQUIREMENTS	C-1
D.	CHALLENGES	D-1
E.	BIBLIOGRAPHY	E-1

List of Figures

Figure 2-1 Mode field diameter.....	2-6
Figure 2-2 Construction of a bare fiber.....	2-8
Figure 2-3 Critical angle.....	2-11
Figure 2-4 Types of polarization maintaining (PM) fiber	2-12
Figure 2-5 WT-bR structure.....	2-24
Figure 2-6 Halobacterium salinarium	2-25
Figure 2-7 bR photocycle.....	2-26
Figure 2-8 Molar absorptivity of WT-bR	2-27
Figure 3-1 Experimental setup.....	3-3
Figure 3-2 Micro-optical components	3-5
Figure 3-3 Beam shape on PLDS-PSPD.....	3-6
Figure 3-4 WT-bR on glass slide	3-11
Figure 4-1 Polarization	4-6
Figure 4-2 WT-bR.....	4-9
Figure 4-3 Bimetallic photoinduced bending.	4-10
Figure 4-4 Photoinduced bending.....	4-11
Figure 4-5 Cantilever upside down.....	4-12
Figure 5-1 WT-bR and PDAC modeled as a spring network	5-7
Figure 5-2 PDAC molecular structure	5-8
Figure B - 1 Side 1	B-1
Figure B - 2 Side 2	B-2

Figure B - 3 Side 3	B-3
Figure B - 4 Side 4	B-4
Figure B - 5 Housing.....	B-5
Figure B - 6 Top plate.....	B-6
Figure B - 7 Bottom plate	B-7
Figure B - 8 Optics trench.....	B-8
Figure B - 9 Translation plate	B-9
Figure B - 10 Experiment	B-10
Figure B - 11 PLDS	B-11
Figure B - 12 Inside the PLDS.....	B-12
Figure B - 13 Inside the PLDS without translation plate.....	B-13
Figure B - 14 Translation plate	B-14
Figure B - 15 Optical components	B-15

List of Tables

Table 2-1 Physical data for the cantilever.....	2-19
---	------

Chapter 1

1 Introduction

Sensor and actuator development are important to nanotechnology.

Nanotechnology is the study of the design, control, and manipulation of devices on the nanometer length scale. To drive sensor and actuator motion, light could be used as the initiator of motion by using photoactive molecules. Many devices exist that convert light to energy in the form of useful work. A few examples of these devices are optical traps¹, optical memory², and more recently the control of the optomechanical cycle of a single molecule³. Upon absorption of a photon by a photoactive molecule, it can go through a conformational change². The coupling between motion and incident light and its effect on the surroundings is of interest.

In 1959 during Richard Feynman's talk "There's Plenty of Room at the Bottom" (given at the annual meeting for the American Physical Society (APS)), he discusses the potential for "...controlling and manipulating things on a small scale". Because of his vision, he helped bring the field now known as nanotechnology to the attention of many scientists at the time. In the years that have past since Richard Feynman's talk, great strides have been made towards the realization of tiny devices either through biological means or other approaches. Knowledge of photoactive molecules has existed for hundreds of years such as the chelate known as chlorophyll, which undergoes a noncyclic and cyclic photophosphorylation (synthesis of ATP from ADP and phosphate resulting from absorbed energy) as an endergonic reaction (absorbs energy from its surroundings)⁴.⁵ A chelate is a metal ion bonded to organic molecules. For chlorophyll the metal ion is magnesium whereas for the heme group of hemoglobin the metal ion is iron. Another

form of photoactive molecule was discovered in the early 70's known as wild-type bacteriorhodopsin (WT-bR), which produced a step towards the construction of tiny devices. The WT-bR molecule undergoes a cyclic (reversible) photophosphorylation that is photokinetic (light induced motion) for the endergonic reaction as opposed to the noncyclic photophosphorylation for the photosystem II of chlorophyll. The process for WT-bR is similar to the process for the photosystem I of the chlorophyll molecule; however, the reaction of the photosystem I for chlorophyll is not a photokinetic process. Furthermore, the respiration process for chlorophyll is enhanced by operating the photosystem I and II in series. Photosystem I is a phototropic (able to react to light in a definite way) system that undergoes a cyclic electron transport that only produces ATP. Whereas, the photosystem II undergoes non-cyclic electron transport that oxidizes water and reduces NADPH (Nicotinamide Adenine Dinucleotide Phosphate Hydrogen: the reduced form of NADP [an enzyme (protein used to catalyze a specific biochemical reaction) that accelerates the removal of hydrogen from metabolites (substance essential to metabolism) and its transfer to other substances])^{6,7}.

Since the endergonic reaction of the WT-bR molecule produces a controllable conformational change that is cyclic, the molecule is an ideal candidate for small devices. In addition, duality of the respiration (both aerobic and anaerobic) for the light-adapted molecule makes it functional in a variety of environments. Therefore, photoactive molecules may provide a means of control and manipulation at a small scale and, hence, push nanotechnology forward. However, the force of interaction between a small device and its environment is important.

In 1986, Binnig et al.⁸ invented the Atomic Force Microscope (AFM), which is capable of measuring the force of interaction between a cantilever tip and a sample. Employing an AFM, the molecular force regimes of photoactive molecules have been previously investigated^{3, 9, 10}. In 1997, Rousso et al. employed a modified version of the AFM known as Near-field Scanning Optical Microscope (NSOM), in which the cantilever of an AFM is replaced by a cantilevered optical fiber⁹. A pulse of electromagnetic radiation, from a Nd:YAG or Dye Laser, was delivered through the fiber to the photoactive sample and the deflection of the optical fiber was measured. Three years later, Periske et al. employed the AFM as a tool to measure the conformation (change in shape of a molecule caused by rotation about a single bond) of photoactive molecules in solution. They illuminated their molecules through a fluid cell, via a halogen lamp¹⁰. Most recently, Hugel et al.³ report the force applied by the optomechanical cycle of a single-molecule by attaching a single-molecule to the AFM tip and to a glass microscope slide. They employ a total internal reflection method to deliver light via a mercury lamp to a photoactive molecule. Although light has been delivered to photoactive molecules in a variety of formats, we know of no format to exist that delivers a pulse of light to the sample from beneath.

Therefore, this thesis will discuss a prototype device known as the Pulsed Light Delivery System (PLDS), which we designed, constructed, and tested. The PLDS can deliver a pulse of electromagnetic radiation directly to the tip-sample interface of an AFM and will thereby allow the study of the mechanical coupling of photoactive molecules to the environment. In order to convey the contents of this thesis, the chapters

are organized as follows: background related to the experiment, the experiment, the results, discussion, and finally the conclusions and future work.

Chapter 2

2 Background

Before discussing aspects of the experiment it would be useful to touch on a few subjects related to the implementation of our apparatus. This chapter is not intended to be all-inclusive (as it would require many volumes of information) for each of the subjects; however, it is intended to inform the reader of enough information to study the coupling of photoactive molecules to the environment. The chapter subsections are organized as follows: (1) paraxial approximation, (2) fiber optics, (3) optics, (4) photoinduced and chemical-induced cantilever deflection, and (5) photoinduced molecular conformations.

The PLDS is a fiber optic coupled box containing many micro-optical components. Hence, the first three subsections will relate to the optical design of the PLDS. The fourth subsection will be connected to an effect caused by the laser being located beneath the cantilever tip. Finally, the fifth subsection is directly connected to the photoactive molecules employed during experimentation.

2.1 Paraxial approximation and Snell's law

The paraxial approximation refers to an assumption for light behavior through an optical system. Therefore, an appropriate place to start is Maxwell's equations, which describe the interaction of light with its surroundings. To show that propagating light behaves as a wave, we assume electromagnetic radiation exists and is traveling isotropically through a material that has a spatially constant permeability and susceptibility with the absence of free charges and currents. Hence, Maxwell's equations are:

$$\nabla \cdot \vec{B} = 0, \tag{2.1}$$

$$\nabla \cdot \bar{\mathbf{D}} = 0, \quad (2.2)$$

$$\nabla \times \bar{\mathbf{E}} - \left(\frac{\partial \bar{\mathbf{B}}}{\partial t} \right) = 0, \quad (2.3)$$

$$\nabla \times \bar{\mathbf{H}} - \left(\frac{\partial \bar{\mathbf{D}}}{\partial t} \right) = \bar{\mathbf{J}}. \quad (2.4)$$

The constitutive relations are:

$$\bar{\mathbf{J}} = \sigma \bar{\mathbf{E}}, \quad (2.5)$$

$$\bar{\mathbf{B}} = \mu \bar{\mathbf{H}}, \quad (2.6)$$

$$\bar{\mathbf{D}} = \epsilon \bar{\mathbf{E}}. \quad (2.7)$$

Substituting the constitutive relations into Eqn. (2.4) one finds

$$\nabla \times \bar{\mathbf{B}} = \mu \epsilon \frac{\partial \bar{\mathbf{E}}}{\partial t} + \mu \sigma \bar{\mathbf{E}}. \quad (2.8)$$

Therefore the wave nature of the electric field component to the electromagnetic radiation becomes evident when crossing Eqn. (2.3) with the ∇ operator and substituting in Eqn.

(2.8) ($\sigma=0$ for an optical system)

$$\nabla^2 \bar{\mathbf{E}} + \mu \epsilon \frac{\partial^2 \bar{\mathbf{E}}}{\partial t^2} = 0. \quad (2.9)$$

The wave nature of the magnetic component of the electromagnetic radiation is completely analogous to the electric, in that, following a similar process for the magnetic component another wave equation is found. If we now assume that the electric field is proportional to a slowly varying component in space multiplied by a rapidly varying component in time and then substituting this into Eqn. (2.9), we find the Helmholtz equation

$$\nabla^2 \mathbf{E} + \mu \epsilon \omega^2 \mathbf{E} = 0, \quad (2.10)$$

where $k = \sqrt{\mu \epsilon} \omega = 2\pi / \lambda$.

The paraxial approximation assumes that a wave of electromagnetic radiation consists of rays of light and that those rays of light do not vary much from the center of the optical components that they traverse. The origin of the paraxial approximation arises from considering the electromagnetic radiation as a plane wave traveling in the z-axis direction, where the electric field component is proportional to

$$\mathbf{E} \sim \psi(x, y, z) e^{-ikz}. \quad (2.11)$$

Substitution of (2.11) into (2.10) results in

$$\frac{\partial^2 \psi}{\partial x^2} + \frac{\partial^2 \psi}{\partial y^2} + \frac{\partial^2 \psi}{\partial z^2} - 2ik \frac{\partial \psi}{\partial z} = 0. \quad (2.12)$$

However, if the source of light is from a laser beam that has a definite direction, there is very little variation of the rays of light from the center of the z-axis. Therefore, the second order differential with respect to z can be set equal to zero. The resulting differential equation is the paraxial parabolic wave equation

$$\frac{\partial^2 \psi}{\partial x^2} + \frac{\partial^2 \psi}{\partial y^2} - 2ik \frac{\partial \psi}{\partial z} = 0. \quad (2.13)$$

Solving the differential equation results in a solution proportional to the Hermite ($H_m(x)$, $H_n(y)$) polynomial. The Hermite polynomials determine the vibrational or modal (TEM_{mn}) distribution of the electric and magnetic components of the electromagnetic field as it is transmitted through the medium.

When the radiation of a laser for a given mode of propagation strikes an interface of a different medium three outcomes are possible. The first is that the wave is reflected.

Second is that the wave is refracted. Finally, the wave could be both reflected and refracted. Without application of any type of special coatings, glass can both reflect and refract when an electromagnetic wave is perpendicularly incident at a plane interface of glass and air. A more general way to write the form of the electric field is

$$E = E_0 e^{ik \cdot x - i\omega t} = E_0 e^{ikx \sin(\theta) - i\omega t} \quad (2.14)$$

At the interface between two different media the phase of the electric field will be the same for the incident, reflected, and refracted wave. Setting the phase factors in the exponential part of equation (2.14) equal to each other, Snell's law is

$$k_i \cdot x = \sqrt{\mu_i \epsilon_i} \omega \cdot x = k_r \cdot x = \sqrt{\mu_r \epsilon_r} \omega \cdot x \rightarrow n_i \sin(\theta_i) = n_r \sin(\theta_r), \quad (2.15)$$

where n_i = index of refraction for the incident medium, n_r = index of refraction for the refracted medium, θ_i = angle of incidence, θ_r = angle of refraction. For an air and glass interface the index of refraction for the incident wave and the reflected wave are the same. Therefore, the angle of incidence equals the angle of reflection. If the variation of a laser beam is negligible along the z-axis and if the incident beam of an optical system is as close to parallel as possible to the optical axis ($\partial^2 \psi / \partial z^2 \sim 0$), the paraxial approximation is valid. Furthermore, it is assumed that the propagating laser beam is Gaussian (see Figure 2-1).

2.2 Fiber optics

Fiber optics have become increasingly important in everyday life. Optical fibers are employed in many different fields such as communication and medical applications. An optical fiber is nothing more than a really tiny glass tube. Of course, it can be plastic too,

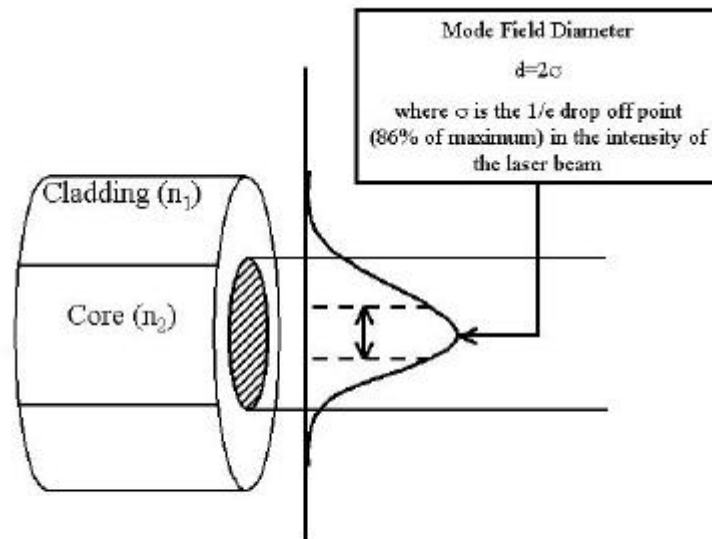


Figure 2-1 Mode field diameter.

As a beam propagates down an optical fiber it has the shape of a Gaussian beam. The mode field diameter is defined to be the point where the irradiation drops off by $1/e$, which gives a rough estimate of the spot size of a beam propagating down an optical fiber.

but in general the better fibers are glass. A fiber is composed of a core, which is typically made of glass, a cladding of higher index of refraction, and an acrylate protective coating; this is what is known as the bare fiber (see Figure 2-2)^{11,12}. Typically fiber optics used in laser systems, communications, and other applications have an additional protective coating known as furcation. The furcation consists of a thin plastic tube, Kevlar™ threads for reinforcement, and an outer plastic coating. The main function of the furcation is to protect the bare fiber from damage.

A beam of light can be transmitted down a cylindrically shaped optical fiber many kilometers before amplification is required. The acceptance cone of rays (NA- Numerical Aperture) that the fiber will accept is calculated from the critical angle required for total internal reflection. Total internal reflection occurs when the incident and reflected light are in a medium of higher index of refraction than the refracted light. When this condition is met and when the angle of incidence has a specific value, the incident light will propagate down the cylindrical tube of an optical fiber, since the core of the optical fiber has a higher index of refraction than the cladding. From Snell's law the critical angle is

$$\theta_c = \sin^{-1} \left(\frac{n_{\text{clad}}}{n_{\text{core}}} \right), \quad (2.16)$$

where θ_c = critical angle for total internal reflection, n_{clad} = index of refraction in the cladding, and n_{core} = index of refraction of the core. However, in order to use the critical angle to calculate the numerical aperture one must know the index of refraction for the glass inside the core and cladding. In general the Numerical Aperture (NA) of an optical fiber is (see Figure 2-3)

$$\text{NA} = \sqrt{n_{\text{core}}^2 - n_{\text{clad}}^2} = n_{\text{core}} \sqrt{1 - \sin^2 \theta_c} \quad (2.17)$$

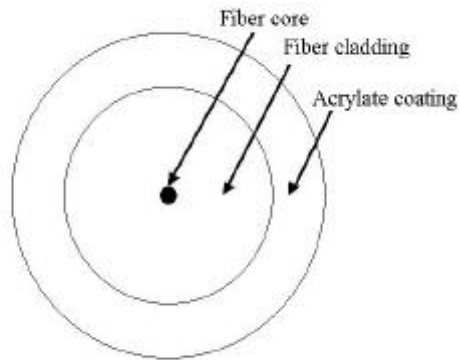


Figure 2-2 Construction of a bare fiber.

Generally, all optical fibers have three main parts to them (the core, the cladding, and the coating). When an optical fiber is “made” the process is called “drawing the fiber” or a “fiber draw”. One could think of the process like trying to pull cheese from a hot pizza. As the hot pizza is withdrawn from one’s mouth there will be strands of cheese running from your mouth to the pizza that will get thinner as the pizza gets further from your mouth. The fiber is typically made of silica (glass) and when heated will form similar strands when there is tension on the heated rod of glass. The stretched strands are cooled and immediately spooled into rolls as the strands of fiber are drawn from the heated rod of glass.

Many different types of optical fibers exist. Two basic classifications are multi-mode and single-mode fiber. Multi-mode fiber allows many modes of the light to propagate; whereas, single-mode fiber only allows one mode to propagate. In addition to the different modes of fiber, there are different types of polarization maintaining (PM) fiber. The types of PM fiber are bow tie, panda, and elliptically clad fiber (see Figure 2-4). The different names of PM fiber arise from the shape of the cladding. The cladding consists of boron-doped glass, which does not allow energy to couple across the core. In other words, the polarization maintaining fiber creates a birefringence (double refraction of the light causes the production of plane polarized light) between the fast and slow axis. The fast axis refers to the transverse electric component and the slow axis refers to the transverse magnetic component of the electromagnetic wave propagating down the optical fiber.

Many ways exist to join optical fibers together. The first way to connect fiber is known as splicing^{13,14,15}. Splices are used to connect the ends of two bare fibers together. This is done by either fusion techniques or mechanical techniques. The mechanical technique is simpler in concept but more difficult to perform. The core of the fibers that are to be connected must be aligned perfectly and, then, refractive index-matching glue cements the two fibers together. Aligning them perfectly without the use of expensive alignment equipment is not possible for very small core diameters, which can range from 0.003 mm to about 1.10 mm. Any slight misalignment between the fiber cores will cause loss of the light propagating down the fiber, since light will be scattered at the interface. Adding to problems of alignment in the mechanical splice, the end of the fibers can be prepared two different ways. If the fiber end faces are parallel to one another, the polish

type is known as a flat cleave. However, if the fiber end faces are at some angle with respect to the optical axis, the polish type is known as an angled cleave. The angled cleave is difficult to perform. Although, there will be less back reflection of light with the angled cleave.

In addition to mechanical splicing, fusion splicing is also used to connect two bare fibers together. Fusion splicing is the easier to use and gives the best results, if the application allows and provided the equipment is available (a typical fusion splicer costs about \$25,000). First, the two fibers that are to be connected are flat cleaved. Then, the fibers are placed in a machine that produces an arc discharge of electricity. The short discharge of electrical energy across the gap of the two fibers causes them to melt. Next, the machine pushes the fibers together so that they are mated (fused) together. Power losses of 0.2 dB or less are easily achievable with this process. The loss of power in an optical fiber is defined as (see Appendix A)

$$\text{dB}_{\text{loss}} = 10\text{Log}\left(\frac{P_i}{P_f}\right), \quad (2.18)$$

where dB = decibel, P_i = Power input, P_f = Power output. The unit of decibel is often used when discussing the performance of a fiber optic system because the values (in dB) for power losses at each component are additive. For example, if a fiber optic system consists of a fiber optic coupler and fiber optic acoustic optical modulator (AOM) with 3 dB (50% Loss) and 2.5 dB power losses, respectively, then the total power loss would be 5.5 dB; the sum of each component in the system. That maximum amount of power throughput (0 dB) using the fusion method is achieved when the flat cleave is properly made, the core of the fibers are aligned within the machine, when there is just the right amount of arc-discharge, and when the fibers are pushed together for the right period of

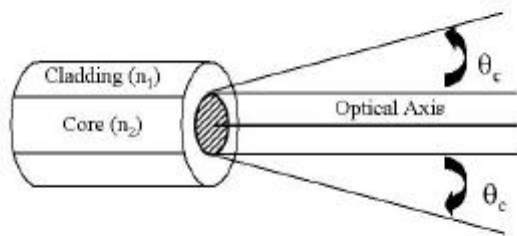


Figure 2-3 Critical angle.

The definition of the critical angle, which is related to the numerical aperture by equation (2.17).

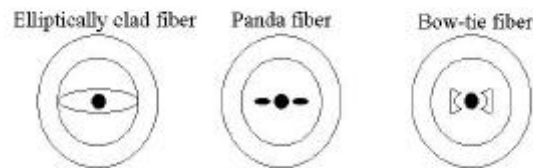


Figure 2-4 Types of polarization maintaining (PM) fiber

The different names of PM fiber arise from the shape of the cladding. The cladding consists of boron doped glass, which does not allow energy to couple across the core. Thereby, the fast and slow axes of the core propagate at different speeds, due to the stress-induced birefringence of the cladding, allowing the polarization to be maintained. The fast axis refers to the transverse electric component and the slow axis refers to the transverse magnetic component of the electromagnetic wave propagating down the optical fiber.

time. The machine parameters (alignment, discharge, and push phase) can be adjusted to induce attenuation at the fiber interface, which makes the machine extremely useful. Attenuators are used to lower the output from a fiber pigtailed laser. For instance, if a laser has four outputs connected to four different laser diodes and the application requires that the output from each leg be identical, an attenuator could be used to attenuate legs higher than the specified output. The most common purpose for splicing two fibers together is to add connectors to the bare fiber.

Another way to join two optical fibers is by the use of connectors. Connectors allow fiber optical components to be connected and disconnected quickly without having to break the fiber, which is a great benefit for any type of fiber optical application where components need to be switched in and out of the system. However, there a lot of different types of connectors, each type serving a particular application. The fiber connector is completely characterized by two pieces of information; the connector and polish type. The most common connectors for laser and telecommunication applications are the fiber connector/angled physical contact (FC/APC) or fiber connector/physical contact (FC/PC). FC/APC connectors have a lower amount of back reflection (~ -70 dB), since the end face of the connector is angled.

The power throughput of an optical fiber is very important. Generally, every effort is made to reduce the amount of back reflection at any interface in the fiber optical system. Despite minimizing the back reflections with correct connection techniques, power losses can still occur between similar types of fiber. When two fibers are spliced together they are not always from the same fiber draw (batch). Although the method of drawing fiber is precise, it still does not guarantee that the core of the fiber is the exact

same size each time it is drawn. Therefore, there can be a mismatch in the core of the fibers causing some light to be scattered at the interface of the connection. Typically, the tolerance for the size of the core is small, so the mismatch in the core size for identical fibers is reduced. However if a larger mismatch occurs, there will be larger attenuation at the fiber interface (provided that the direction of light down the fiber is such that it travels from the smaller core to the larger core). The loss of power in decibels is given by

$$\text{Loss}_{\text{dB}} = 2 \times 10 \log \left(\frac{1}{2} \times \left(\frac{R_1}{R_2} + \frac{R_2}{R_1} \right) \right), \quad (2.19)$$

where R_1 = mode field radius of the first fiber (mode field diameter/2), and R_2 = the mode field radius of the second fiber. If $R_1 \sim 2.5 R_2$, then about 50 percent or 3.0 dB of the light will be lost at the interface. The percentage loss is

$$\% \text{Loss} = 100 \exp \left[- \left(\frac{\text{dB} \times 2.303}{10} \right) \right], \quad (2.20)$$

where dB= value of loss in decibels.

The mismatch in core size between fibers is not the only source for power loss through the fiber optical system¹¹. Some other examples of power loss are the mismatch in types of connectors, the mismatch in core diameters (for both alike and unlike fibers), improper splicing, bends in the fiber (critical angle is no longer satisfied), attenuation due to absorption in the fiber (can be wavelength dependant), improper coupling of the laser light into the fiber (NA is too high). Furthermore if the laser is pulsed, broadening of the pulse width can occur from dispersion, which occurs when the fast and slow axes propagate at different speeds. However as in the case of the polarization maintaining fiber, the fast and slow axes are designed to have some dispersion, since the refractive

index is different between the polarization axis and the axis rotated $\pi/2$ from the polarization axis.

2.3 Optics

Electromagnetic radiation is completely characterized by Maxwell's equations, the constitutive relations, the Lorentz force equation, and the continuity equation. However, using a computer to calculate the form of an electromagnetic wave after it passes through a number of different components requires complicated software because Maxwell's equations must be solved with the correct boundary condition at each interface. To simplify the process, two methods have been developed that easily lend themselves to computer analysis. One method is known as Ray Tracing (RT) and the other is known as the Gaussian Beam Propagation (GBP) method^{16,17,18}. These methods are known as geometrical and are entirely equivalent to solving the Maxwell equations at each interface.

Ray tracing a paraxial ray is performed by tracing rays of light through an optical system. The goal is to determine the formation of an image by balancing aberrations such that the real rays converge to the same image point as the paraxial rays. This method is numerical in nature and is used to optimize the difference between real and paraxial rays by employing a matrix method to describe the solution to a system of equations.

It is useful to show the form of the equation describing the general form of a wave governed by the paraxial approximation in order to describe the GBP method. Using Eqn. (2.11) and substituting into Eqn. (2.13) and then solving

$$\psi(x, y, z) = \frac{w_0}{w(z)} H_m \left(\frac{\sqrt{2}}{w} x \right) H_n \left(\frac{\sqrt{2}}{w} y \right) \exp \left[-i(kz - \phi(z)) - r^2 \left(\frac{1}{w(z)^2} + \frac{ik}{2R(z)} \right) \right], \quad (2.21)$$

where w_0 = constant spot-size of the beam, $w(z)$ = radial amplitude distribution, $r^2=x^2+y^2$, and $R(z)$ = radius of curvature of wave front. Therefore, the Gaussian beam is completely characterized by the specification of any two of the following parameters z , $R(z)$, w_0 , $w(z)$.

Fortunately, there is a simple relation for calculating the minimum spot-size expected from an optical system. The relation is proportional to the wavelength of light and the F_{number} of the last lens in the system. The F_{number} is inversely proportional to the diameter of the lens and directly proportional to the effective focal length of the lens (F_{number} = effective focal length / diameter of the lens). Therefore, the expected spot size, a , is calculated from

$$a = \left(\frac{4\lambda}{\pi} \right) F_{\text{number}} = \frac{1}{2\text{NA}}, \quad (2.22)$$

where NA stands for the numerical aperture.

2.4 Photoinduced and chemical-induced cantilever deflection

Photoinduced^{19,20,21,22,23,24} and chemical-induced^{25,26,27} cantilever deflections have been reported by a number of groups. With the capability of measuring subnanometer (~0.2 nm for our instrument) deflection, uses for microcantilevers in sensor-based nanotechnology are possible. The deflection of the cantilever can be caused by (to mention only a few possibilities) light, motion of a small particle or a system of particles, thermal dissipation into a system, or a combination of effects. In 1994, J. R. Barnes et al.²³ reported that silicon microcantilevers could be used as a calorimeter or thermometer. Most silicon microcantilevers are purchased with a reflective coating to help reflect the positioning laser off the back of the cantilever. The reflective coating is typically some type of reflective metal such as gold or aluminum. Assuming there is a thin layer

(~50nm) of aluminum coating on top of the silicon cantilever, it will bend when heated due to the mismatch in thermal expansion coefficients between silicon ($\alpha_2 = 3 \times 10^{-6} / ^\circ\text{C}$) and aluminum ($\alpha_1 = 25 \times 10^{-6} / ^\circ\text{C}$), which is known as the bimetallic bending effect²⁸.

The cantilever is assumed to be a rectangular beam. The other assumptions are that the temperature varies uniformly from top to bottom, one end is hanging freely, the other end is fixed, and the cantilever is heated at the free end. Additional assumptions for the bimetallic beam (cantilever): (1) The beam material is homogenous with the same modulus of elasticity in tension and compression. (2) The beam is nearly straight (if there is a slight curvature, it is in the plane of bending and the radius of curvature is at least 10 times the depth. (3) The cross section is uniform. (4) The beam has at least one longitudinal plane of symmetry. (5) All loads and reactions are perpendicular to the axis of the beam and lie in the same plane, which is a longitudinal plane of symmetry. (6) The beam is long in proportion to its depth, the span/depth ratio being 8 or more. (7) The beam is not disproportionately wide. (8) The maximum stress does not exceed the proportional limit (the point on a stress-strain diagram after which Hooke's law is not valid)²⁹. Then the general differential equation describing the deflection of a rectangular beam is^{23,29}

$$\frac{d^2z}{dx^2} = \frac{M}{EI}, \quad (2.23)$$

where z = vertical deflection of the cantilever, M = the bending moment equation, E = modulus of elasticity, and I = area moment of inertia about the centroid axis of beam cross section. In general, equation (2.23) is complicated by form of the bending moment

equation. If we follow the assumptions for the cantilever and then solve equation (2.23) the result for the maximum deflection can be cast in the following form²⁹

$$z(0) = 3(\gamma_1 - \gamma_2) \frac{t_1 + t_2}{t_2^2 K} (T - T_0) L^2, \quad (2.24)$$

where L = length of the cantilever, $z(0)$ is the deflection of the end of the cantilever t_1 = thickness of aluminum layer, t_2 = thickness of silicon, γ_1 = thermal expansion coefficient of Al, γ_2 = thermal expansion coefficient of Si. Note (see Table 2-1),

$$K = 4 + 6 \left(\frac{t_1}{t_2} \right) + 4 \left(\frac{t_1}{t_2} \right)^2 + \frac{E_1}{E_2} \left(\frac{t_1}{t_2} \right)^3 + \frac{E_2}{E_1} \left(\frac{t_2}{t_1} \right), \quad (2.25)$$

where E_1 , E_2 are Young's moduli for the aluminum and silicon, respectively.

One additional piece of information, which may be useful, is the thermal relaxation constant

$$\tau = \frac{L^2 (\rho_1 C_1 t_1 + \rho_2 C_2 t_2)}{2 (\lambda_1 t_1 + \lambda_2 t_2)}, \quad (2.26)$$

where ρ_1 = density of aluminum, ρ_2 = density of silicon, C_1 = heat capacity of Al, C_2 = heat capacity of Si, λ_1 = thermal conductivity of Al, and λ_2 = thermal conductivity of Si.

Using the data in Table 2-1 and taking the max deflection to be the limit of our instrument (0.2 nm) and solving Eqn. (2.24) for the temperature change, the temperature sensitivity is calculated to be 1.50×10^{-3} K per unit division (0.2 nm or 1 mV for our instrument) and the time constant for thermal relaxation is 0.71 ms.

More recently, A. Subramanain et al.²⁷, report on a chemical-induced deflection of a silicon microcantilevers. By coating the cantilever with an enzyme and placing it in contact with glucose, an exothermic reaction takes place causing the cantilever to be heated, which in turn causes the cantilever to bend. The assumptions for the bimetallic

	Aluminum (Al)	Silicon (Si)	
Thickness (t_1, t_2)	50.0 nm	1.95 μm	
Young's modulus (E_1, E_2)	70.0 GPa (10^9 N/m^2)	47.0 GPa (10^9 N/m^2)	
Thermal expansion coefficient (γ_1, γ_2)	$24 \times 10^{-6}/\text{K}$	$2.6 \times 10^{-6}/\text{K}$	
Heat capacity (c_1, c_2)	905 J/kgK	705 J/kgK	
Thermal conductivity (λ_1, λ_2)	237 W/mK	141 W/mK	
Density (ρ_1, ρ_2)	2700 kg/m^3	2330 kg/m^3	
Cantilever length (L)			350 μm
Cantilever width (w)			35 μm
Minimum deflection $z(0)$			0.2 nm
Bandwidth for data acquisition			1 MHz

Table 2-1. Physical data for the cantilever

Physical data for the cantilever (bimetallic beam) used to calculate the change in temperature per unit division.

beam (cantilever): (1) The difference between thermal expansion coefficients is constant during heating. (2) Friction at the support can be neglected. (3) The width of the beam is very small³⁰. They predict the change in temperature to be

$$\Delta T = \frac{h \left[3 \left(1 + \frac{t_1}{t_2} \right)^2 + \left(1 + \frac{t_1}{t_2} \left(\frac{E_1}{E_2} \right) \right) \left(\left(\frac{t_1}{t_2} \right)^2 + \frac{1}{\left(\frac{t_1}{t_2} \right) \left(\frac{E_1}{E_2} \right)} \right) \right]}{6(\gamma_1 - \gamma_2) \left(1 + \frac{t_1}{t_2} \right)^2} \frac{2z}{L^2 + z^2}, \quad (2.27)$$

where h = cantilever thickness. Both equations (2.24) and (2.27) give the same result for the temperature change per unit voltage (or nanometer). The only difference between Eqn. (2.24) and (2.27) is that Eqn. (2.27) has the term on the right side that was meant to correct for a bending curve arc. However, the ratio of the correction term to the $z(0)$ (since $z(0)=z$) divided by L squared term for Eqn. (2.24) is identical. This makes sense when one notices that in the ratio for the two terms, the z term drops out and since z is much less than L the ratio becomes 1 (indicating the equations are similar).

2.5 Photoinduced molecular conformational changes

Wild-type bacteriorhodopsin (WT-bR) is a naturally occurring protein contained within a purple membrane that is found in *Halobacterium Salinarium*, which was discovered in the early 70's. WT-bR is well-studied and understood molecule that occurs naturally in salt marshes². The work that has been done on WT-bR in the past has included measurements from SEM³¹, x-ray diffraction³², neutron diffraction³³, STM³⁴, and AFM³⁵.

Additionally, WT-bR occurs in a hexagonally packed two-dimensional crystal, which makes it stable. *Halobacterium Salinarium* has evolved to live in rough

environments by surviving using either aerobic or anaerobic (corresponding to phototrophic (bacteria that uses light for growth and derives its carbon from carbon dioxide) behavior) respiration. The efficiency to convert sunlight to chemical energy by WT-bR is about 15%, which is about half as efficient as a chlorophyll system (~35% conversion)³⁶. Chemical energy refers to the potential energy stored in the chemical bonds formed during an endergonic (absorbs energy from the surroundings) reaction.

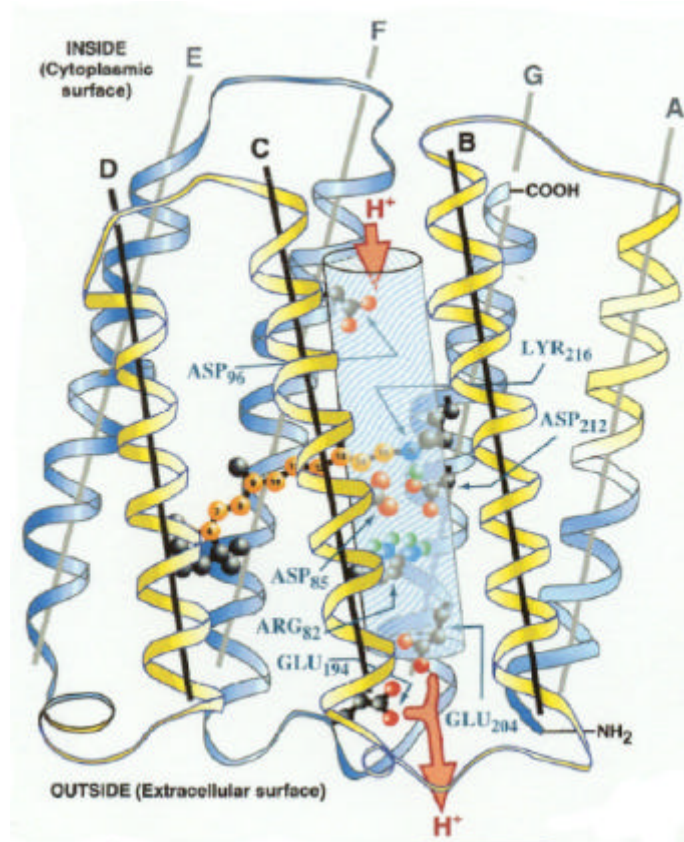
The molecule consists of a chain of 248 amino acids. At the center of WT-bR is a proton pump, which pumps a proton from the cytoplasmic side to the extracellular side of the molecule (see Figure 2-5 and Figure 2-6). The movement of the proton corresponds to a cyclic behavior of the molecule resulting from photostimulation, where the cyclic behavior is known as the photocycle of WT-bR (see Figure 2-7)³⁷. The molecule can pump as many as 100 protons per second. Full sunlight (~ 15 mW/area²) will not saturate the molecule. At the center of the proton pump is a chromophore that is an all-trans retinal, which is bound to a lysine as a protonated Schiff base (A compound formed by a condensation reaction between an aromatic amine and an aldehyde or ketone.)². The surrounding part of the molecule is an enzymatic catalyst.

Upon absorption of one or two photons at the chromophore (chain of carbon atoms formed as a conjugated double bond) two subpicosecond processes occur; the first is an excitation to the Franck-Condon excited state (HOMO to LUMO transition) causing a shift in the electron charge density within the molecule, around the C13=C14 carbon bond, and the second is the delocalization of the primary charge carriers, pi electrons³⁸. A delocalized electron arises when a molecule that has a string of conjugated double bonds

(polyene), which is a single bond followed by a double bond, is created. The double bond results in the pi-orbital becoming covalently bonded to the next conjugated double bond. Hence, an electron has equal probability to be in any of the pi orbitals along a conjugated chain and is therefore free to move about the chain, which is referred to as being delocalized. One way to think of this is that the entire chain of conjugated bonds is a superposition of each of the pi orbital wave functions for each individual carbon atom. The relocalization of the pi electrons causes a reorganization of the nuclei for bacteriorhodopsin; however, the nuclei are not able to shift as quickly as the charge density, since they are much more massive than the electrons. Therefore, the reorganization of the nuclei lags the shift in electron charge density.

Once the nuclei are in their new equilibrium positions, the molecule has undergone a conformational change. Initially in the configurational state (all-trans) or ground state (BR), the atoms for the double bond about the 13th carbon position are transversely situated about the symmetry axis (all-trans). After excitation, the atoms around the double bond are orientated adjacent to each other about the plane of symmetry (13-cis) otherwise known as the M state. Once these processes occur, the system decays nonradiatively to the ground state via phonon emission, while transporting a proton from the cytoplasm to the extracellular space. There are a number of intermediate steps in between the ground state and excited state, however the BR to M transformation is the primary initiator of conformational change³⁸. The conformation is differentiated by a height extension of about 2 Angstroms³⁹. The entire cycle is reversible and decays thermally every 5 milliseconds. In addition, only a single protein is needed to convert light energy into chemical energy. In the next section, we delineate the device we intend

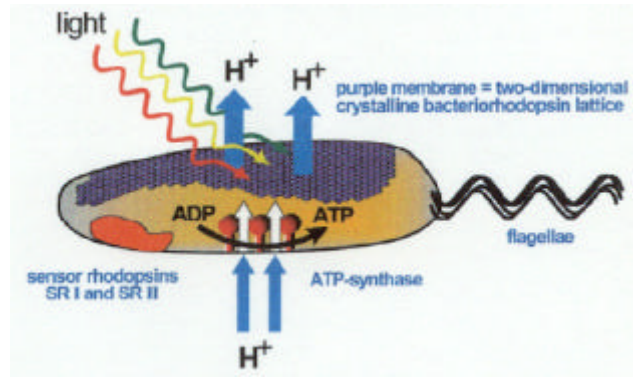
to use as a tool to measure the transfiguration of the BR molecule from all-trans to 13-cis. The unique behavior of bacteriorhodopsin makes it or a derivative of it a viable material for use in nanotechnology devices. Some possible uses for bR are photovoltaic converters, super fast detection, motion detection, artificial retinas, or high-energy radiation detection. Capitalizing on the photocycle, there have been many patents for bR related devices, the earliest being awarded in 1980. Currently, the Japanese have 60, the United States have 20, and the European countries have 10 patents³⁶.



From reference: 2

Figure 2-5 WT-bR structure

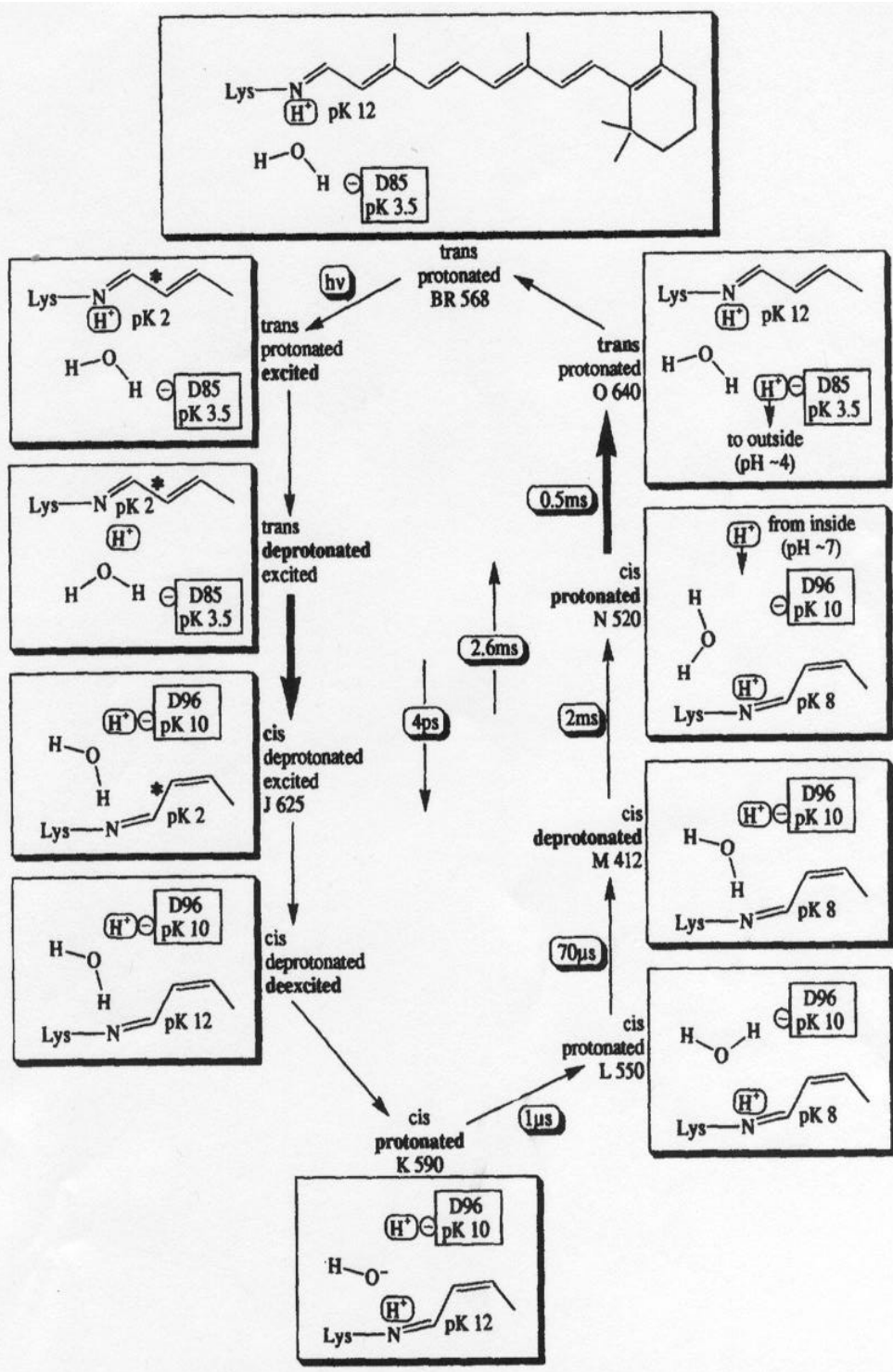
The tube at the center is the proton pump. The A-G helical shaped ribbons refer to the seven trans-membrane α -helices of the secondary structure. The all-trans retinal is covalently bonded to LYS-216 through a protonated Schiff base. The orange spheres are carbon atoms.



From reference: 36

Figure 2-6 Halobacterium salinarium

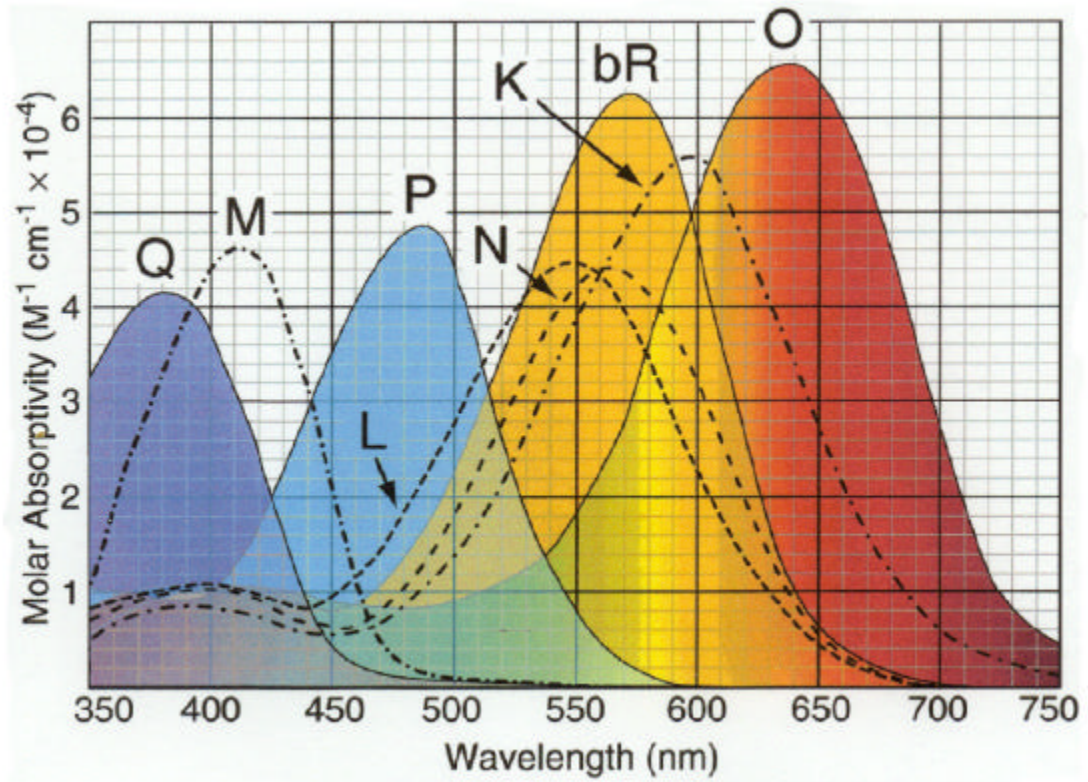
A proton is transported from the cytoplasmic to the extracellular side, which creates an electrochemical gradient that the bacterium uses to make ATP (adenosine triphosphate: stores energy to be used in endergonic {absorbs energy from its surroundings} reaction). The rhodopsin sensors are used to sense whether the correct wavelength (to initiate the photocycle) is present, which triggers the flagellae motor (to move the bacterium into the light).



From reference: 37

Figure 2-7 bR photocycle

This chart represents the intermediate states throughout the WT-bR photocycle.



From reference: 2

Figure 2-8 Molar absorptivity of WT-bR

The different types of dashed lines distinguish the absorptivity between the various photointermediates.

Chapter 3

3 Experimental Methods and Apparatus

3.1 Apparatus

The experimental arrangement is depicted in Figure 3-1 (see also Appendices B and C). The system consists of a fiber coupled frequency doubled continuous wave Nd:YAG laser operating at a wavelength of 532 nm, purchased from B&W Tek. The laser is connected to an Acousto-Optical Modulator (AOM), capable of operating in continuous wave (CW) or pulsed mode, via an SMF-28™ jumper cable. The AOM was purchased from NEOS Technologies allowing us to deliver pulses with a 70 nsec rise and fall times over a 40 MHz bandwidth. The AOM is fiber pigtailed into single-mode polarization maintaining fiber. The output of the AOM is connected to about 10 m of additional single-mode polarization maintaining fiber. The end of the 10 m of fiber has a flat cleave, which is used to bring light to the pulsed light delivery system (PLDS; see Figure 3-2). The other end is coupled to the AOM via a FC/PC (Fiber Connector/Physical Contact) connector. Within the PLDS is an optical system consisting of two different legs of micro-optical components. In-house construction meant that the device could be built quickly and cheaply.

The first leg of the PLDS is designed to transport the radiation to a sample of photoactive molecules and the second is designed for alignment and focusing purposes. The first leg contains a ball lens (BL), a polarizing beam splitter (PBS), a reflecting right angle prism (P), a quarter-wave plate (QWP), and finally a lens (L). Initially, the beam of photons exits the flat face of the single-mode fiber and enters the ball lens, where the diverging beam is collimated (diameter = 2.0 mm). Next, the beam moves to the

polarizing beam splitter where only the transverse electric field component, which is parallel to the plane of incidence and perpendicular to the direction of propagation, known as the primary wave (PW), is transmitted. If the beam is not plane polarized, the perpendicular or the transverse magnetic component, known as the secondary wave (SW), is reflected by the polarizing beam splitter. After traversing the PBS, the plane polarized light becomes circularly polarized, which is caused by the quarter-wave plate. Immediately following, the beam is focused onto the plane of the sample by a lens with a focal length of 6.0 mm (diameter = 3.0 mm).

Once the beam is transmitted from the lens of the first leg to the reflective cantilever tip (through a hole drilled in the top plate of the PLDS) and if the tip is above the beam spot, it will be reflected. The reflected light returns back through the lens, through the quarter wave plate (changing the circular polarization to linear polarized light along the secondary axis), then to the prism where it is reflected down the secondary leg. Next, the beam is routed through another lens that focuses the light onto a cylindrical lens, which focuses on the photodetector. An increase in total voltage from the photodiode means that the cantilever tip is over the top of the spot. Since the shape of the cantilever tip is conical, the incident light on the tip will be reflected at differing angles, so it is possible that no light will be reflected back through the system.

In order to adjust the focus of the beam in the object plane (sample), the lens and QWP are fixed to a plate that can be moved 1 mm, constrained to move along the z-axis only. The change in height of the plate along the z-axis causes a displacement in the focusing plane towards (or away from) the object plane depending on whether the lens is moved up or down. The plate is translated by turning a nut on a threaded rod that the

Location	Power Loss (dB)
Jumper Cable	0.7
AOM	2.5
Fiber cleave	2.3
PLDS	3.5

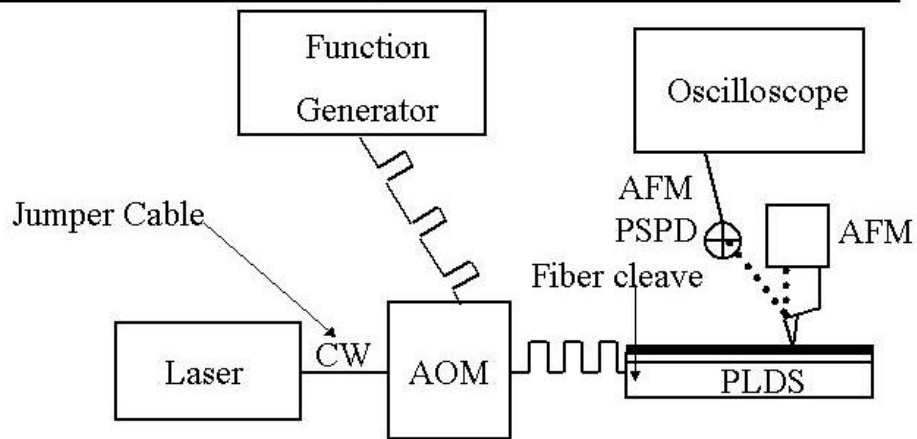


Figure 3-1 Experimental setup

The laser ($\lambda=532\text{nm}$) operates in CW mode. The AOM, connected to the laser via an SMF-28 jumper cable, turns on when the voltage is high and off when it is low. The function generator produces pulses with a 10 ms cycle time and delivers them to the AOM. The PLDS is connected to the AOM by an FC/APC connector. The PLDS delivers the light pulses to the shaded area, which is the sample, and the motion of the cantilever is detected by the AFM-PSPD. The oscilloscope reads the voltage from the AFM-PSPD and records the average of 256 periods. As a note, the PLDS is able to fit within the AFM because the instrument scans the cantilever as opposed to the sample. The table indicates the amount of power loss at different points within the experimental setup.

plate rests on. Then the shape of the reflected light provides useful information. The cylindrical lens causes astigmatism, which causes a change in the beam shape at the PLDS-PSPD (pulsed light delivery system-position sensitive photodetector). Astigmatism is an aberration resulting from the difference between the focus of the tangential and sagittal plane. In between the tangential and sagittal plane is the meridional plane. If the lens is translated down along the z-axis, the object plane will be in tangential focus resulting in a horizontally elliptical beam shape. If the lens is translated up along the z-axis, the object plane will be in sagittal focus resulting in a vertically elliptical beam shape. However, if the object plane coincides with meridional focus, the beam shape is circular^{40,41,42}. Since the PLDS-PSPD is a four-quadrant photodetector, the amount of voltage for a given quadrant will determine whether tangential, meridional, or sagittal focus is present by indicating the beam shape. If the beam shape is circular, no translation of the lens plate is necessary. However, for either of the other two types of beam shape the lens plate will need to be translated up (down) if the beam shape is elliptically horizontal (elliptically vertical).

The PLDS housing was fabricated by us, which consists of a box made of black acetal plastic (the color black will allow light to be absorbed so that reflections will be minimized), copper plates for the top and bottom, plastic columns, and a threaded rod and nut. The base of the plastic is milled, so that the optical fiber has a trench to restrict movement and so that the optical components have a place to rest. Three of the sidewalls have a hole in them. One hole is for the delivery of the beam, the second hole is for the z-translation control of the lens, and the third hole is for a four-quadrant position-sensitive photodetector (PSPD). As a note for clarification, there are two different PSPD's. One

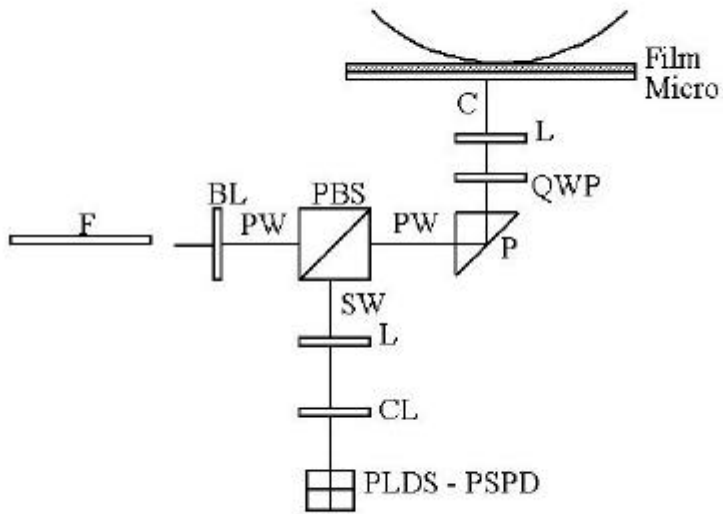


Figure 3-2 Micro-optical components

The micro-optical components contained within the PLDS, which delivers the pulse of light. F=polarization maintaining single mode fiber, BL=ball lens, PBS=polarizing beam splitter, P=prism, QWP= $\lambda/4$ wave plate, L=lens, micro=microscope slide, L=lens, CL=cylindrical lens, PSPD=position-sensitive photodiode. The upper half of the micro-optical components is the first leg (F, BL, PBS, P, QWP, L, Micro). The lower half is the second leg (PBS, L, CL, PSPD). PW= transverse electric component of the electromagnetic field (parallel to the plane of incidence), SW= transverse magnetic component of the electromagnetic field (perpendicular to the plane of incidence), and C=circularly polarized light.

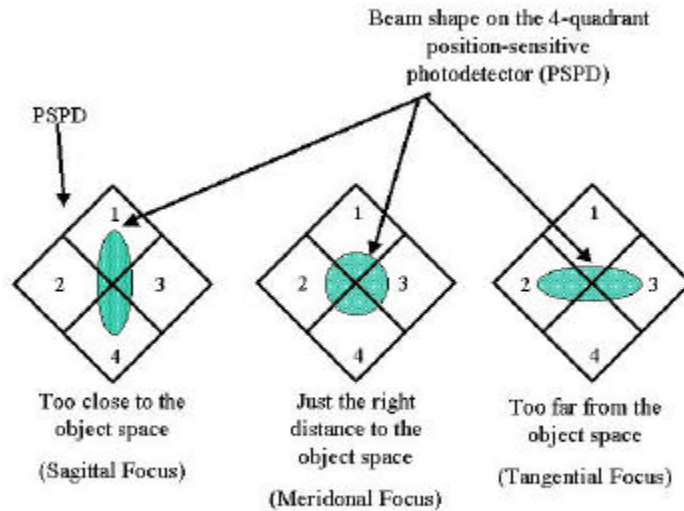


Figure 3-3 Beam shape on PLDS-PSPD

If the focus is perfect, the four-quadrant photodetector will have equal voltages on all diagonals. However, if the focus is not perfect, then there will be a difference in voltage between the diagonals on the PSPD. When the object is too close, addition of the voltages on quadrants 1 and 4 will be higher than the addition of quadrants 2 and 3. If the focus is too far from the object, addition of the voltages on quadrants 2 and 3 will be higher than the addition of quadrants 1 and 4.

belongs to the PLDS and one belongs to the AFM.

The completed PLDS unit has dimensions of 67 by 59 by 21 mm. Since our AFM scans the cantilever tip as opposed to scanning the sample, the entire device will fit between the stage and the suspended cantilever tip. Furthermore, since it is fiber pigtailed the device is easily placed and removed into and out of the AFM. Finally, the microscope slide is fixed to the top of the PLDS by tape.

3.2 Procedure

The optical alignment of the PLDS was performed without the use of fine positioning equipment. The following list describes the process:

1. **PM Fiber Cleave.** The PM fiber (diameter of 125 μm and a core diameter of 6 μm) was cleaved until the power output was maximized and the output had a visible Gaussian pattern.
2. **Optical Axis Alignment.** Aligned the center of the PM fiber core down the optical axis. The micro-optical components were much larger than the core diameter of the fiber allowing for the paraxial approximation to be valid.
 - a. **Fiber Orientation.** Determine the best orientation for the fiber by measuring the output from the fiber through the polarizing beam splitter.
 - i. When the maximum power reading was obtained, the fiber was fixed to the PLDS.
 - b. **Ball Lens.** The ball lens was aligned by positioning it in front of the fiber, such that the smallest visible spot emerged.
 - c. **Beam Splitter.** The beam splitter was relatively easy to place after the ball lens, as long as the correct orientation was maintained.

- d. **Prism.** After that, the right angle reflecting prism proved to be the most difficult to align. The position of the prism must correspond to reflecting the beam upward in a straight a line.
- e. **Second Leg.** Once the first leg was fixed firmly to the PLDS with super glue, the second leg was secured.
- f. **Lens and QWP.** Finally, the remaining components of the first leg and the second leg were aligned in a similar fashion and fixed to the PLDS.

To perform the experiment the following list of steps were developed:

1. **Sample.** We placed an uncoated microscope slide on the PLDS.
2. **Approach.** We approached the surface in contact mode.
3. **Stop Scanning.** We stopped the cantilever ($k=0.03$ N/m) from scanning,
4. **Laser.** We turned the laser on (114 μ s pulses).
5. **Deflection.** We observed the deflection of the cantilever as a function of the time. As a note, the microscope slide was used as the baseline for comparison with the coated slides.
6. **Calibration.** We calibrated the voltage on the AFM-PSPD by measuring the nanometer per unit voltage conversion.
 - a. Align the positioning laser on the back of the cantilever.
 - b. Make contact with an uncoated microscope slide.
 - c. Go to force-curve acquisition mode for the AFM.
 - d. Make sure measure is checked in force spectroscopy mode.
 - e. Click Run.

- f. Adjust the extension and retraction so that steepest part of the force curve covers as much of the plot as possible.
 - g. Read the x and y coordinates at the top and bottom part of the curve.
 - h. Calculate the slope of the curve as nanometer per unit voltage.
7. **Change Sample.** The sample was changed without moving the position of the cantilever detection beam, so as to not change the calibration factor.

The placement of the PLDS using the AFM xy stage was straightforward, but requires explanation:

1. **PLDS.** The PLDS was placed under the hood of the AFM and onto the translatable xy stage.
2. **Sample.** An uncoated or coated microscope slide was immobilized by tape to the top of the PLDS.
3. **Laser.** The laser was turned on in CW mode.
4. **Positioning Laser.** The positioning laser was aligned on the back of the cantilever.
5. **Laser Spot Alignment.** Observing the television monitor, the xy stage was translated in small increments until the cantilever was at the origin of the laser spot exiting the PLDS.
6. **Approach.** As the cantilever was brought in contact with the sample, the Auto-Approach was stopped, periodically, and the xy stage was moved so that the laser spot exiting the PLDS was centered beneath the cantilever. The reason for moving the xy stage as we translated down was a result of the optical misalignment within the PLDS.

3.3 Sample

For the sample, wild-type bacteriorhodopsin (WT-bR) was deposited on a glass slide with an electrostatic technique⁴³ such that there was a definite orientation (see Figure 3-4). The extracellular side was facing the glass and the cytoplasm was facing outward. Since WT-bR was negatively charged, a 1 nm layer thick of PDAC (Polydimethyldiallammonium Chloride) was deposited in between layers of WT-bR, which were 9-10 nm thick. There were three different substrates: a monolayer, a 10 layer, and a 75 layer of WT-bR molecules. If the sample is relatively flat all molecules should move in unison and, therefore, each of the different layers should undergo a conformational change of 0.2 nm, 2 nm, and 15nm, respectively. To measure whether or not a conformation occurred we monitored the cantilever deflection signal, in contact mode, on an Autoprobe M5 AFM from TM Microscopes using an oscilloscope from Agilent (model: 54621D). Employing this method, we expect to see a deflection of the cantilever upwards as evidenced by an increase in voltage. The signal should increase in a picosecond, but then decay back to the equilibrium position exponentially over 10 milliseconds, indicating thermalization back to the ground state³.

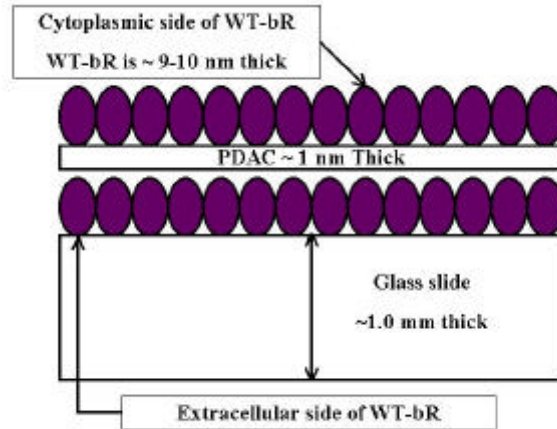


Figure 3-4 WT-bR on glass slide

WT-bR was electrostatically deposited on a glass slide. The extracellular side was facing downward and towards the glass slide and the cytoplasmic was facing upward away from the glass slide. The PDAC was a cation surface added to help deposit the WT-bR. The PLDS delivers light to the extracellular side.

Chapter 4

4 Results

In this section, the performance of the PLDS (pulsed light delivery system) is evaluated (see also Appendices C and D). The specific characteristics of interest are the power throughput, the energy per pulse, the number of photons available for absorption per molecule, polarization, laser spot size exiting the PLDS, how well the optical system is aligned, the surface roughnesses of the uncoated and coated microscope slide, and the amount of cantilever deflection.

4.1 Power

Initially, from the output of the PLDS, we have measured a continuous wave minimum power of $12 \pm 9 \mu\text{W}$ and a maximum of $903 \pm 9 \mu\text{W}$ with a Newport handheld power meter with wand attachment (model: 840C). All data were collected at the maximum power output. Once the experiments were completed an attempt was made to realign the optics, since the fiber and the prism were slightly askew. In order to realign the two micro-optical components, the entire optical system needed to be realigned. In doing so, the final maximum power setting was $427 \pm 10 \mu\text{W}$. The power down the second leg was minimally $12 \mu\text{W}$ and maximally $27 \mu\text{W}$. Placing a mirror over the PLDS produced no detectable increase in the power down the second leg. The misalignment of the optical axis could be askew to the point that the reflected light from the tip does not travel down the second leg. More details of problems with optical axis alignment are found in the Discussion. These problems indicate that the second leg does not, currently, function for focusing purposes. However, the second leg could be calibrated for use as a power meter. Additionally, it is worth noting that the output of the PLDS poses no risk of

damage to the video camera for the AFM. The video camera is similar to the camera that are sold commercially to consumers (which can be used both indoors and outdoors). The reason it is believed that no damage will occur is that direct sunlight during the summer in New England produces a power reading of 15 mW/cm² at the earth's crust, which is much greater than the PLDS output.

4.2 Energy and number of photons delivered

Next, it is important to know how much energy is being delivered to the sample space by the PLDS. To determine the amount of energy delivered to the sample we multiplied the continuous wave power (P_{cw}) by the pulse width (w). The resulting minimum pulse energy was 0.150 nJ for a 12.3 μ s pulse width and the maximal was 362 nJ for a 401 μ s pulse width. Next, comparing how much light is available to how much is needed; we first calculated the energy per photon ($E_{\text{photon}} = hc/\lambda$) as 3.76×10^{-19} J. Then, estimating a PLDS laser spot diameter of 10 μ m ($r_b = 5\mu\text{m}$) and WT-bR with a radius of 5 nm (r_m -per molecule) we divided the areas of these two, resulting in the total number of WT-bR molecules as 1×10^6 . In general, the total number of photons delivered per molecule is

$$\frac{N_{\text{ph}}}{\text{molecule}} = \left(\frac{r_m}{r_b} \right)^2 \left(\frac{w P_{cw}}{E_{\text{photon}}} \right), \quad (2.28)$$

where $r_m = 5.0$ nm, $r_b = 5$ μ m, $P_{cw} = 903$ μ W, $w = 114$ μ s (values used in the experiment).

We expected that there would be 2.74×10^5 photons per molecule delivered. With a 65 percent quantum efficiency we expect that 1.78×10^5 photons would be left after the initial absorption. WT-bR only needs one photon at 532 nm to initiate the photocycle, so the probability is extremely high that the photocycle will commence. The absorption

maximum occurs at 568nm^{37} , so it is likely that quantum efficiency will be less than 65 percent, since we are using light at 532 nm.

4.3 Polarization

To measure the polarization, a polarizer was placed in the path of the output of the PLDS and the power was measured as a function of angle rotated (see Figure 4-1). The polarization data is presented by treating the power measurement as R and the angle as θ , then calculating $X=R\sin(\theta)$ and $Y=R\cos(\theta)$ to create each data point for Figure 4-1. Notice that after realignment the data distribution seems to be more circular than before. Since circular polarization was expected from the PLDS, it seems that circular polarization was improved after realignment.

4.4 Spot size

To measure the spot size of the beam exiting the PLDS, first a cantilever was brought down to within 10 microns of the PLDS. Then, the end of the cantilever was aligned along the edge of the beam shape at the widest point. Next, the x and y positions of the stage were recorded. Afterwards, the stage was translated so that the cantilever end moved in a straight line across the beam shape. Finally, the x and y positions of the stage were recorded again and subtracted from the initial stage positions resulting in the spot size. As a note, the beam was not entirely circular in shape (only the widest point along the x direction was recorded). The cause of the non-circular shape was a result of aberration and misalignment in the optical system.

The minimum achievable spot size before realignment was $47.5\ \mu\text{m}$ at $19\ \mu\text{W}$ and the maximum was $110\ \mu\text{m}$ at a power of $254\ \mu\text{W}$. The minimum achievable spot size

after realignment was 45 μm at 12 μW and the maximum was 70 μm at a power of 427 μW . The calculated minimum spot size, a , is given by:

$$a = \left(\frac{4\lambda}{\pi} \right) F_{\text{number}} , \quad (2.29)$$

where $\lambda = 532\text{nm}$ and $F_{\text{number}} = 2$ (lens closest to sample). Therefore, the minimum spot size should be 1.4 μm . Reasons for the larger measured spot size will be discussed later.

4.5 Alignment

Another important factor in device function is how well the beam is aligned along the optical axis. There is an observable deviation to the propagation of light from the PLDS; therefore, an attempt was made to quantify this amount of misalignment. One technique was to place a mirror over the output. This would reflect the light back through the lens and down the second leg, which could be attached to a photodetector. By determining the amount of light reflected we could determine how well the optical axis was aligned. However, we did not measure any increase in power due to the reflected light. A possible reason could be that the angular deviation of the beam was large. However, we did use another method to make an estimate of the optical alignment. If the optical axis were perfectly aligned, the beam will propagate from the lens and converge to a focal point and then diverge; however, the center should still be along the z-axis without any translation in x or y. The direction cosines for the ideal case should be $\alpha = 90^\circ$, $\beta = 90^\circ$, $\gamma = 0^\circ$. The misalignment did cause a translation in the x and y direction of the beam spot as we translated up along the z-axis. The direction cosines were calculated based on the measured difference in x, y, and z positions (as observed from the AFM software) before the translation and after the translation. The values before

realignment were: $\alpha = 83^\circ$, $\beta = 84^\circ$, and $\gamma = 9^\circ$ and after $\alpha = 83^\circ$, $\beta = 96^\circ$, and $\gamma = 9^\circ$.

Comparing these values for the alignment to the ideal case, it is found that the beam propagates slightly askew.

4.6 Surface roughness

One additional measurement is useful as an indicator as to whether or not we would expect to see a conformational change in the photoactive molecules. The surface roughness of an uncoated microscope slide indicates the corrugation of the surface topography. A low voltage, Topo x 16, 256 x 256, and contact mode image (size: 2 square microns) was taken of the uncoated microscope slides before being coated (surface roughness = 0.5 ± 0.1 nm). Since the conformational change corresponding to the 75-layer thin film should be larger (15 nm) than the surface roughness of the microscope slide (0.5 nm), it was expected that a conformational change would be observed. After the slides were coated, a high voltage, Topography, 256 x 256, and contact mode image (size: 6 x 6 microns, radius of the tip = 47 ± 14 nm [to measure the tip radius, multiple images were taken of a delta function grating and then the radius was calculated using SPMLab™ software for each image]) was taken of the coated microscope slides (see Figure 4-2). However, the root-mean-square fluctuation of the surface roughness for the coated microscope slides were 17, 31, and 31 nm (monolayer, 10 layer, 75 layer respectively). We did not observe any conformational change of WT-bR resulting from the perturbation of the laser beam for all three layers, which was not expected. However, one mechanism was clearly observable the photoinduced cantilever bending.

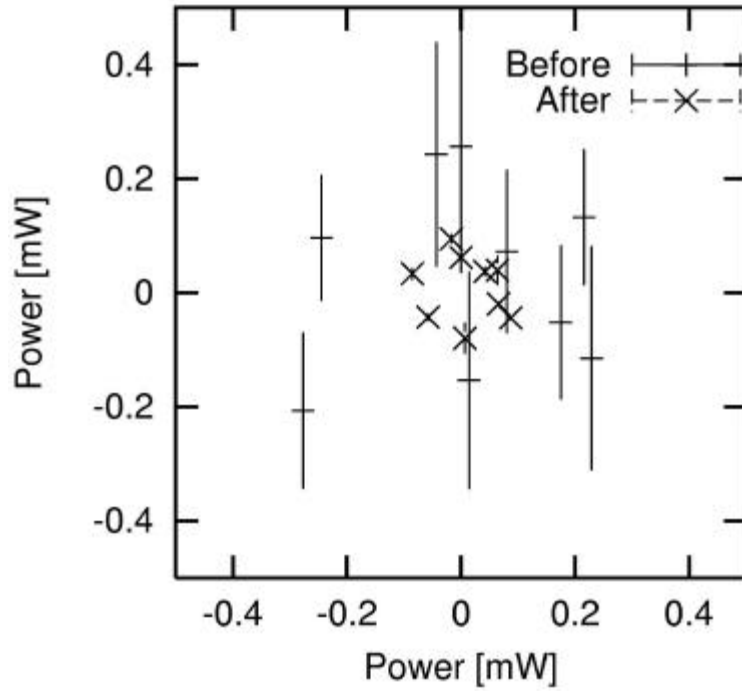


Figure 4-1 Polarization

The polarization was calculated by setting the power measurement at a given angle equal to R and the angle equal to θ . Then, to create each data point $X=R\sin(\theta)$ and $Y=R\cos(\theta)$ were calculated. Notice that after realignment the polarization is much closer to circular, as desired.

4.7 Cantilever deflection

We compared the deflection of a reflective-coated cantilever and of an uncoated cantilever while they were hanging freely (see Figure 4-3). In addition, we observed the cantilever's deflection while a reflective-coated cantilever was hanging freely, while in contact with an uncoated microscope slide, while in contact with a transparent compliant material called Gelpak™, and while in contact with microscope slides coated with WT-bR (Figure 4-4). Datskos et al. have already investigated the bending of a microcantilever and attribute bending of the cantilever from a laser to photogenerated excess free charge carriers and thermal stress²⁴ with the thermal stress being less noticeable. However, we see the thermal stress known as the 'bimetallic' effect²³ (see Figure 4-3). The laser beam causes heating at the end of the cantilever and because of the mismatch in thermal expansion coefficients between the silicon cantilever ($\alpha_2 = 3 \times 10^{-6} / ^\circ\text{C}$) and the aluminum reflective coating ($\alpha_1 = 25 \times 10^{-6} / ^\circ\text{C}$), the cantilever bends downward. The downward trend in the spike corresponds directly with the pulse from a function generator to the Acousto-Optical Modulator. A similar behavior is observed by flipping the cantilever over (see Figure 4-5). However, the effect becomes smaller and the deflection is upward. We anticipated observing a height change with the uncoated cantilever corresponding to a conformational change in the WT-bR samples, which was not observed.

The qualitative behavior of the deflection is the same for a reflective-coated cantilever hanging freely and a reflective-coated cantilever in contact with transparent substrates (see Figure 4-3 and Figure 4-4). The cantilever is relatively stable until the pulse of light strikes the cantilever surface. Once this happens, the cantilever appears to

bend downward, continuously, until the end of the pulse. When the tip is in contact with the sample the cantilever cannot move down significantly. Because the AFM-PSPD is sensitive to the angle of reflection caused by the detection laser bouncing off the reflective part of the cantilever, it is more likely that the end of the cantilever rotates toward the sample around the axis of the tip. Afterwards, the cantilever returns to its original equilibrium position. The minima observed in the peaks of Fig. 5 seem to indicate that the differing values are due to the compliance of the material because of the different layer thicknesses. Notice that the Gelpak™ (no WT-bR) has the same behavior as the WT-bR coated slides. Furthermore, the angle rotated should be lesser for thicker samples (since they are more compliant), which seems to be the trend, except for WT-bR-10.

Despite succeeding at power delivery, problems still exist with alignment and polarization resulting in power loss. In addition, the specific choice for optical components causes a greater than expected maximum spot size. The following section will discuss issues associated with this study.

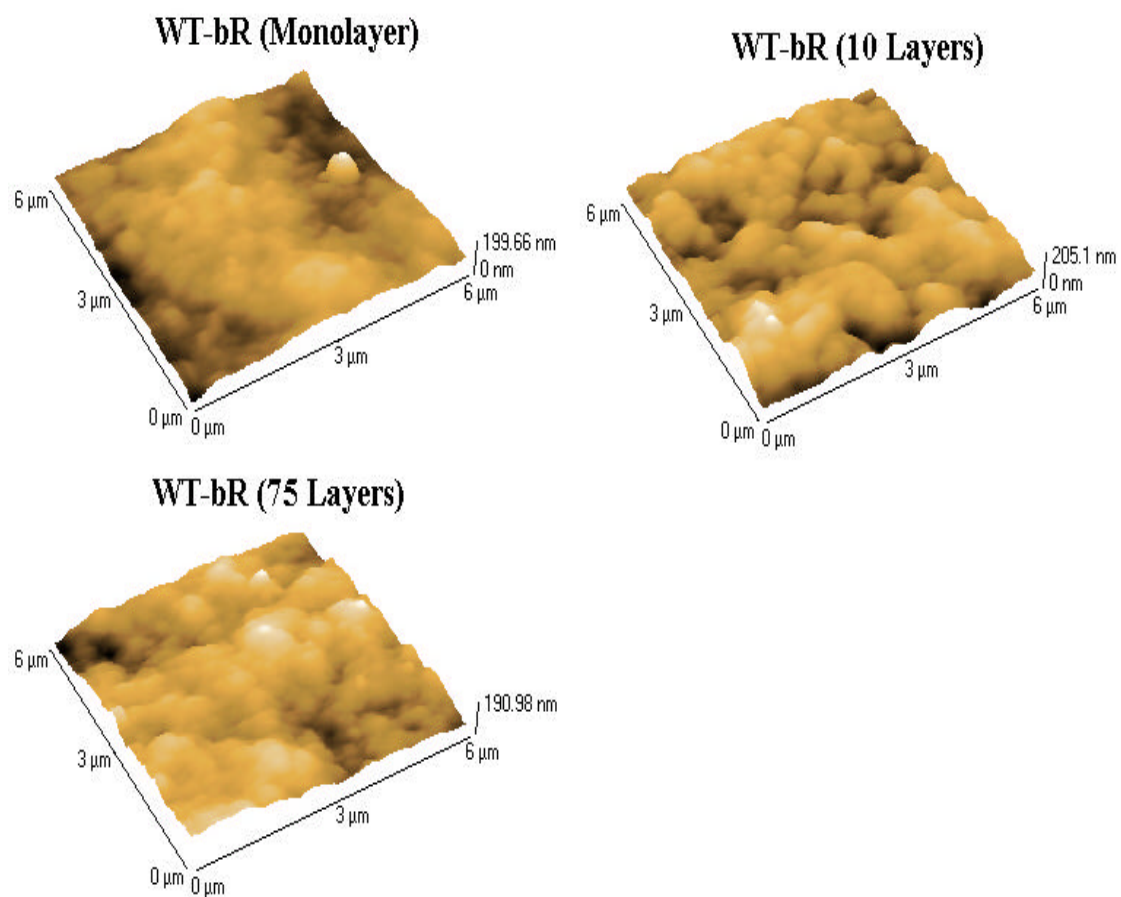


Figure 4-2 WT-bR

The above is an AFM topography image of the sample photoactive molecules. (Image parameters: high-voltage, 256 x 256 pixels, contact-mode, tip radius = 47 ± 14 nm, $k = 0.15$ N/m).

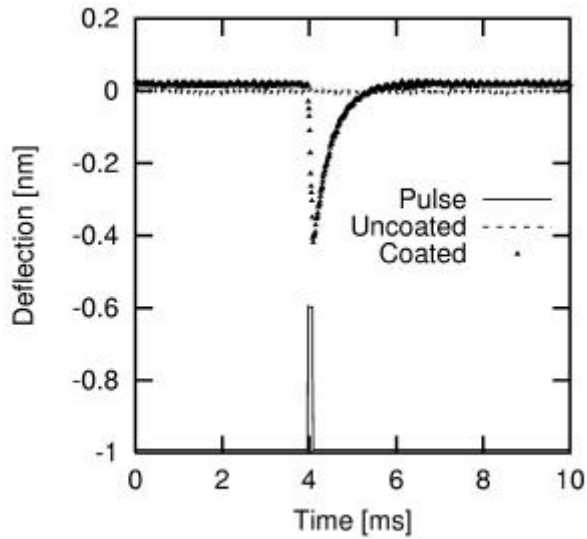


Figure 4-3 Bimetallic photoinduced bending.

The uncoated cantilever ($k=0.30$ N/m) does not have the reflective aluminum coating, whereas the coated cantilever ($k=0.35$ N/m) does. The data were taken while the cantilever was hanging freely in air. Dividing by 100 and then subtracting a small DC offset (0.05), the voltage pulse to the AOM becomes visible on the same graph as the cantilever deflection. Notice there is no cantilever deflection when the cantilever is uncoated. In addition, the relaxation time was determined by calculating the time in milliseconds the cantilever took to return back to the equilibrium point after being perturbed. The average relaxation time for the above deflection was 1.7 ms. Note, this value is close to twice the calculated relaxation time of 0.71 ms. However, this seems to indicate that the relaxation time as calculated by Eqn. (2.26), should not assume that the cantilever is heated only at the end. Rather if the equation were to assume that the temperature of the cantilever were constant along the length then the time constant would be increased by a factor of 2, resulting in better agreement with the experiment.

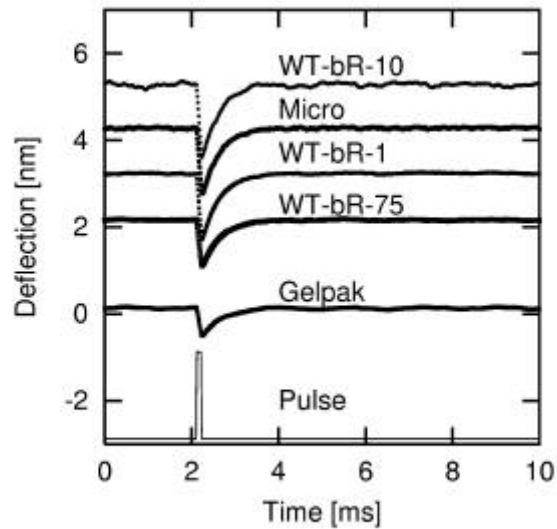


Figure 4-4 Photoinduced bending.

The cantilever deflection data were taken while in contact with the respective sample.

The cantilever deflection data were offset by a small DC value (increments of 0.05), in order to view the individual curves better. Dividing by 25 and then subtracting a small DC offset (0.1), the voltage pulse to the AOM becomes visible on the same graph as the cantilever deflection. In addition, the relaxation time was determined by calculating the time in milliseconds the cantilever took to return back to the equilibrium point after being perturbed. The average relaxation times for the above deflections were 1.4 ± 0.5 ms.

Note, this value is twice the calculated relaxation time of 0.71 ms. However, this seems to indicate that the relaxation time as calculated by Eqn. (2.26), should not assume that the cantilever is heated only at the end. Rather if the equation were to assume that the temperature of the cantilever were constant along the length then the time constant would be increased by a factor of 2, resulting in better agreement with the experiment.

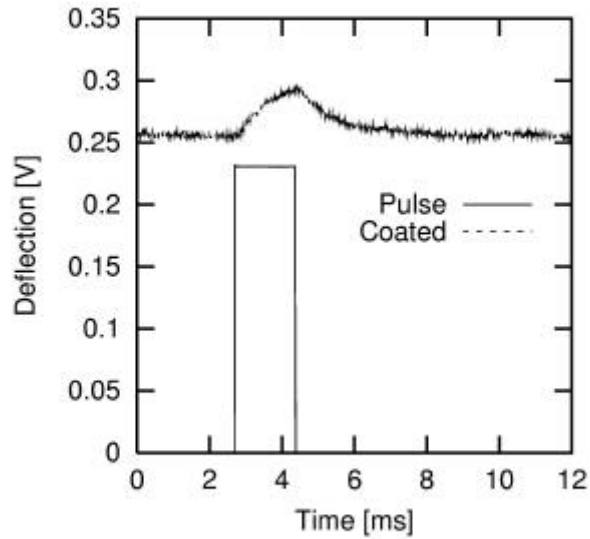


Figure 4-5 Cantilever upside down.

The cantilever ($k = 0.03 \text{ N/m}$) was flipped over when it was placed in the cantilever holder. The data were taken while the cantilever was hanging freely in air. In addition, the relaxation time was determined by calculating the time in milliseconds the cantilever took to return back to the equilibrium point after being perturbed. The relaxation time for the above deflection was 2.7 ms. Note, this value is larger than the calculated relaxation time of 0.71 ms. It is not clear as why this is so much larger.

Chapter 5

5 Discussion

In this chapter, we will delineate any important points related to the experiment not previously mentioned. The organization of the subsections will be broken into the two following categories (1) the PLDS performance and (2) the sample of photoactive molecules.

5.1 PLDS performance

Power throughput is an important factor in the delivery of light. Initially, when the fiber pigtailed laser was built for us, SMF-28™ fiber was used. At our operational wavelength that fiber is multimode and is not polarization maintaining. Being not polarization maintaining, the fast and slow axis will not propagate the energy at the same speed, causing a small shift in phase at the output of the laser. The small shift in phase means the light will not be perfectly linearly polarized, which means some light will be lost in the reflection down the second leg of the PLDS. Furthermore, the AOM is fiber pigtailed into single-mode polarization maintaining fiber with FC/PC (Fiber Connector/ Physical Contact) connectors, but the fiber from the laser is multimode and not polarization maintaining with FC/APC (Fiber Connector/ Angled Physical Contact) connectors. So an SMF-28™ jumper cable was purchased that has an FC/PC connector on one side and an FC/APC connector on the other side. This solves the problem of the mismatch in connectors at the AOM; however, there will be power loss due to the mismatch in fiber core. The core mismatch at the interface of the jumper cable and the AOM translates into a large loss of power and scales as the core area of the jumper cable divided by the core area of the AOM fiber squared. The phase shift caused by the SMF-

28TM fiber was partially corrected for by winding the fiber tightly and rotating the fiber until the power throughput of an analyzer was minimized along an extinction axis. The solution is very similar to a polarization controller in that it causes a stress-induced birefringence. Hence, there will be additional power loss tangent to the winding. Another source of power loss comes from the intrinsic operation of the AOM. Furthermore, the fiber cleave must be flat to reduce stray light, so if it is not perfectly flat it could cause leakage of light, which would result in loss of some power.

More sources exist for power loss, such as the scattering of light and the optical axis misalignment. Alignment was performed by hand and eye by maximizing the amount of power throughput through each micro-optical component. The total diameter of the fiber is 125 microns and the core 6 microns. Ideally for maximum throughput, the optical axis would be directly aligned with the core of the fiber. The size of the core is not visible by eye. However, maximizing the power will give an indication that we are as close as possible to the optical axis, without directly observing the alignment of the fiber core. Invoking the paraxial approximation meant that the micro-optical components could be misplaced along the optical axis by no more than ± 200 microns. Extremely fine hand movements were required to align the micro-optical system, which was a very difficult task to perform within the tolerance. The power losses (in decibels) at various locations of the experimental set-up are found in the table of Figure 3-1.

The spot size variation was larger than we expected; the reason may be due to spherical aberration introduced at the ball lens. In the future, spherical aberration could be reduced with the use of an achromatic lens and by first expanding the beam so that the F_{number} could be reduced.

5.2 Sample

The conformational change of WT-bR was not observed, which was not anticipated. The samples of WT-bR had patches of molecules dispersed throughout the slide, with some being larger than others. An attempt was made to find a local maximum within a six-micron square grid, but this does not necessarily mean that the location was 1 layer, 10 layers, or 75 layers thick.

Additional problems may exist with the sample. The tip was much wider than the molecules. If a cantilever deflection were observed, it would be a statistical average ensemble of all molecules moving underneath the tip. One could imagine that some molecules were stacked higher and some lower than others and that the surface of the tip was a series of peaks and valleys (similar to dimples on a golf ball, but possibly less uniform). If the difference in height between the higher stacked and lower stacked molecules is large enough (for example ~ 10 nm difference), the higher stacked molecules could make contact with the cantilever tip whereas the lower stacked ones may not. Furthermore, one could imagine that the higher stacked molecules might make contact at a localized peak on the cantilever tip and that once conformation is initiated the molecule could slip into a nearby valley on the cantilever tip causing the cantilever to be deflected only after the slipping motion. Hence, the slipping motion would cause a lower average height (by ~ 1 - 2 nm). However, since conformation was not observed it is not clear that this effect will matter.

Further complications could occur in the choice of cantilever stiffness. A higher stiffness could deform the surface and reduce the motion of the molecules. However, interatomic forces can range from 10^{-7} N (for ionic bonds) to 10^{-12} N (for hydrogen

bonds)⁸. To a first approximation we could consider Hooke's law as applicable and, therefore, make an estimate for an appropriate value for the stiffness (of the cantilever). If we assume a deflection of 15 nm (the amount expected for the 75-layer of WT-bR), then the force gradient, corresponding to the intra-molecular bond, should be about 67 N/m for the strongly bound case and 6.7×10^{-4} N/m for the weakly bound case. If we assume a deflection of 0.2 nm (the amount expected for the monolayer of WT-bR), then the force gradient, corresponding to the intra-molecular bond, should be about 5000 N/m for the strongly bound case and 0.05 N/m for the weakly bound case. Assuming that the covalent bonding within WT-bR falls somewhere in the midrange for stiffness (~30-2500 N/m), the stiffness of our cantilever was low (0.03-0.3 N/m), so as to not deform the sample. Note, that this was an oversimplification of what might be happening for multiple layers of WT-bR and PDAC. One could imagine that the stacked molecules are actually stacked springs, with the spring constant being different for the WT-bR and PDAC molecules. However, one could assume that the stiffness is the same (statistical average) between different molecules of WT-bR and PDAC (see Figure 5-1).

The statistical average corrugation (randomly alternating ridges and grooves) on the surface of the microscope slide could be important. The rougher the slide the more uneven the thin film layer. Fortunately, the corrugation is on the order of angstroms for the uncoated slide, so it is unlikely that the roughness (or corrugation) would cause an uneven film surface. An effect should be observed but it should be small compared to the change in height with respect to the 75-layer film. However, the RMS (Root Mean Square) deviation (a measure of the deviation from the average roughness of a surface) of the 75 layer of WT-bR was measured to be 31 nm, which is greater than the expected

height change of 15 nm. Furthermore, the roughness of the monolayer of WT-bR molecules is larger than the expected overall thickness of the film. The expected thickness of a single layer should be on the order of 10 nm; however, the measured roughness was 17 nm. A possible reason for measuring a larger surface roughness than the expected thickness for WT-bR would be that the monolayer was not a monolayer in the region scanned, but perhaps a bi-layer or more of molecules were deposited. Additionally, the unusually high deviation of the surface roughness may indicate that our films were not as well ordered as expected.

Finally, one more reason we may not see any conformational change results from film depositing technique. Jin-An He et al.⁴³ report on an electrostatic technique to assemble multiple layers of bacteriorhodopsin. The glass microscope slide has a polycation surface and WT-bR is negatively charged. A single monolayer will easily adsorb to the glass slide, actually up to 4 layers will adsorb. However, in order to continue layering a polycation material, known as PDAC (Polydimethyldiallylammonium Chloride) is added in between layers of WT-bR. As a side note, the ionic strength or pH of the PM must be adjusted to provide enough Columbic force to adhere to the PDAC. The first main issue is that the compliance of this PDAC material is unknown. One could imagine that these layers of PDAC could act very efficiently as shock absorbers, reducing the motion of the molecules. If these polycation layers were compliant enough, no observable motion would occur.

We could estimate how compliant (since compliance is related to the bond energy) the PDAC might be as compared to the WT-BR by calculating the enthalpy (or bond energy, or disassociation energy, or bond strength) to break the bonds of the atoms

in each molecule. A chain of 16 carbon atoms is primarily responsible for the conformational change in WT-bR. Eight of the carbon pairs are double bonds (bond energy = 682 kJ/mol) and seven are single bonds (bond energy= 348 kJ/mol). Therefore, the total energy (in units of kJ/mol) required to rip apart the entire chain is $7(348)+8(682) = 7892$ kJ/mol. Following a similar method to break apart all the atoms in the PDAC the bond energy is found to be 10250 kJ/mol (see Figure 5-2). Since the bond strength (or energy) is smaller for the WT-bR molecules than the PDAC, it is expected that the PDAC may not be more compliant than the WT-bR. If the assumptions for the calculations are correct, there is no clear understanding as to why we did not see any conformational changes. As a side note, the disassociation energy was assumed to be the sum of all the disassociation energies for each bond that had to be broken. In reality, there may only be one or two bonds that are of most importance in each molecule that affect the stiffness. For, instance the double bond at the 13th and 14th carbon is the pivot for rotation of the conformational change of WT-bR. Therefore, it may be best to compare the disassociation energy for this double bond to some pivotal point in the structure of the PDAC (either within the structure of the PDAC or at the interface (electrostatic coupling) between the PDAC and the WT-bR). However, the pivotal point is not known, so no further comparison was made.

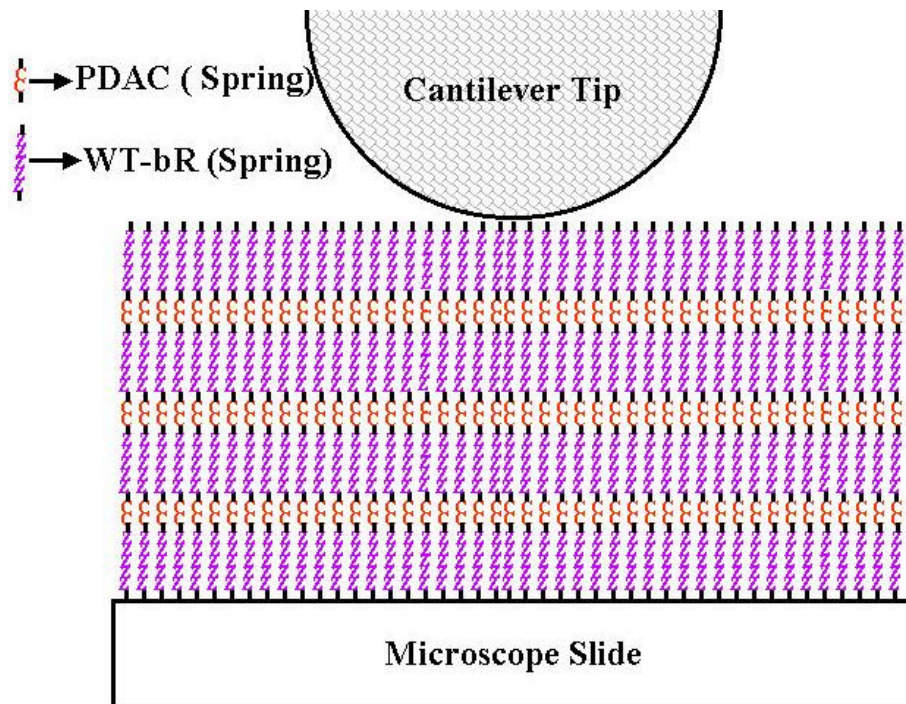


Figure 5-1 WT-bR and PDAC modeled as a spring network

The sample layers of WT-bR and PDAC could be modeled as a continuous link of coupled harmonic driven oscillators. One could complicate the model by assuming that the spring constant for each molecule is different and that the motion may not be constrained to the z-axis only. For instance the molecules could be constrained to move only along the z-axis close to the microscope slide but allowed to rotate about the z-axis in the xy plane at some location closer to the cantilever tip. One could throw many proverbial “wrenches” into the system that would cause solving for the motions or stiffnesses to become quite complicated. One additional assumption someone might expect is to assume that the springs are not rigidly connected to either the microscope slide, to each other, or both within some interaction distance.

- single bond
= double bond

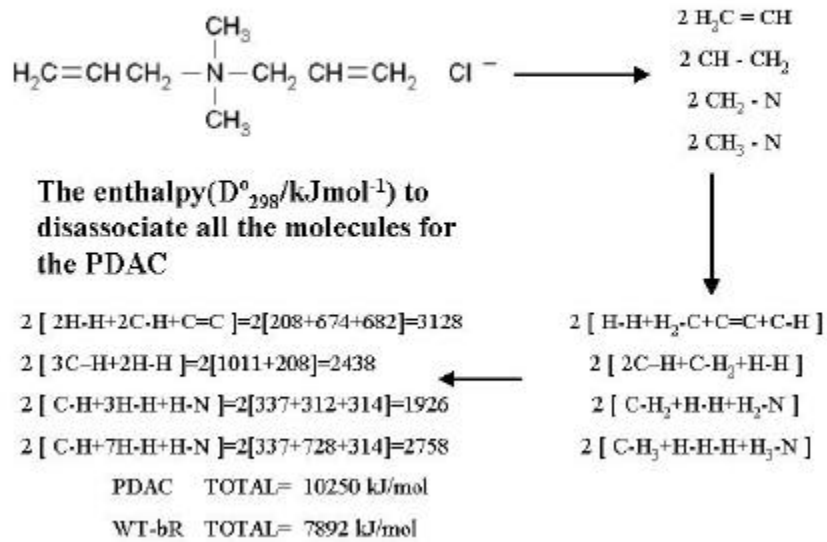


Figure 5-2 PDAC molecular structure

To determine the disassociation energy for a molecule, one needs only determine the energy to break the bonds between constituent parts within the molecule. One might expect that not all bonds have to be broken in order to dramatically effect the structure of the molecule. Therefore the above disassociation energy may be a gross overestimation of the bond energy for this molecule.

Chapter 6

6 Conclusions and future work

Concluding, we have shown that the PLDS, which we designed and constructed, can deliver a pulse of light to the tip-sample interface of the AFM. Figure 4-3 and Figure 4-4 show the cantilever deflection as a function of time and it is clearly visible that enough energy in the form of electromagnetic radiation was delivered through the sample to cause a photoinduced bimetallic bending of the reflective-coated cantilever.

To increase the power throughput, substitution of the SMF-28™ fiber for another fiber that is polarization maintaining would reduce the amount of interface loss between the SMF-28™ fiber and the polarization maintaining single-mode fiber of the AOM. Besides the mismatch in the cores, the slightly multimode fiber of the SMF-28™ causes the laser light to be only partially linearly polarized. This partially polarized light causes additional losses at the polarizing beam splitter, since both the PW and SW exist before the beam splitter. However, if the light were truly linearly polarized there would not be losses at the beam splitter.

In the future, improvements could be made to the design and construction of the PLDS. However, this version represents the best possible configuration with what was available. Ideally, modeling a pulse of light through the PLDS and photoactive molecules to the cantilever tip would be beneficial. The model would optimize the parameters (power, pulse width, and type and position of micro-optical components for a given sample of molecules) and thus will reduce the likelihood of multiple constructions. Also, the part should be fabricated in the machine shop with better quality control over the positioning of the micro-optical components. Precision alignment components exist, but

not on a length scale that will fit into the AFM. Further development of these components would be necessary to the overall development of the PLDS.

Another suggested improvement is a result of not observing any conformational change. Care must be taken so that the sample of photoactive molecules adhere to certain requirements. The requirements for the photoactive molecules are 1) a measurable component of the conformational change must be orientated along the z-axis, 2) the change in height of the molecule must be much higher than the noise level of the AFM (much greater than 0.2 nm), and 3) the addition of compliant layers (employed to induce deposition of the molecule) must be minimized (possibly replace the PDAC with a stiffer molecule).

Two last suggestions: (1) (although enough energy is getting through the sample to cause a photoinduced motion of the cantilever) since the spot size is large, there may not be enough power delivered to the sample for the given area of molecules. However, if the power values are correct then there should not be an issue with too little power to initiate the photocycle of WT-bR. Switching to a different photoactive molecule that is larger in diameter, has a much higher (than 0.2nm) conformational change, and requires one green (532 nm) photon to initiate the photocycle may provide a more fruitful experience. (2) Since low humidity can affect the thermal stability of WT-bR, the sample molecules may need to be in a more humid environment⁴⁴.

Appendix

A. Decibel

The decibel was named after Alexander Graham Bell and is a tenth of a bel. One bel is defined to be $P/P_0=10$ where P is the power output and P_0 is the power input. The level of a power quantity in units of bel is defined to be $\log(P/P_0)$. In decibels, the level of a power is defined as $10\log(P/P_0)$. Note this should not be confused with the level of a field quantity as defined for circuits to be $20\log(V/V_0)$ (in units of decibel) where V is the final voltage and V_0 is the initial voltage. The factor of 2 arises when one considers that the power in a circuit is $P = I^2R = V^2/R$, the factor of 2 comes down out of the logarithm to multiply the level of a power quantity to make it a level of a field quantity (for further clarification see section 8.7 of the NIST (National Institute of Standards and Technology) web page <http://physics.nist.gov/Pubs/SP811/sec08.html>).

Appendix

B. Sketches and photographs

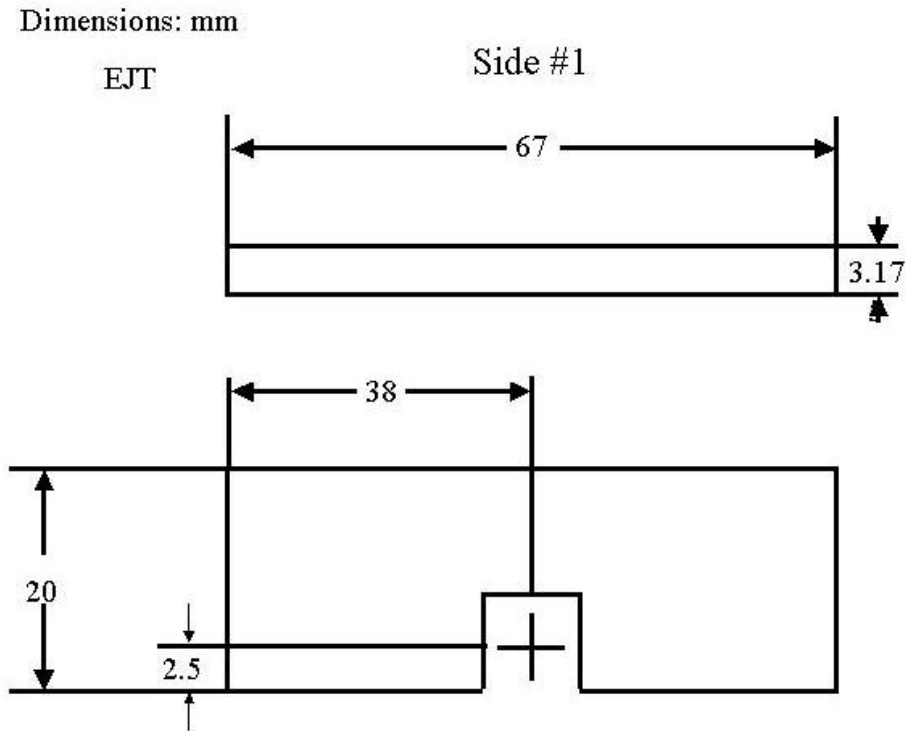


Figure B - 1. Side 1

Side 1 (made of black plastic) contains the position sensitive photodiode for the pulsed light delivery system. Plastic is adequate since we have a low power laser. In order to use a high power laser anodized metal must be used. The PLDS has six walls altogether. The walls were glued together to form a box. However, the top of the PLDS was fixed to the PLDS by screws, so that it could be removed. The ability to remove the top allows the user to adjust the micro-optical components within. In general, the micro-optical components are fixed in place (with the exception of the translation plate).

Dimensions: mm

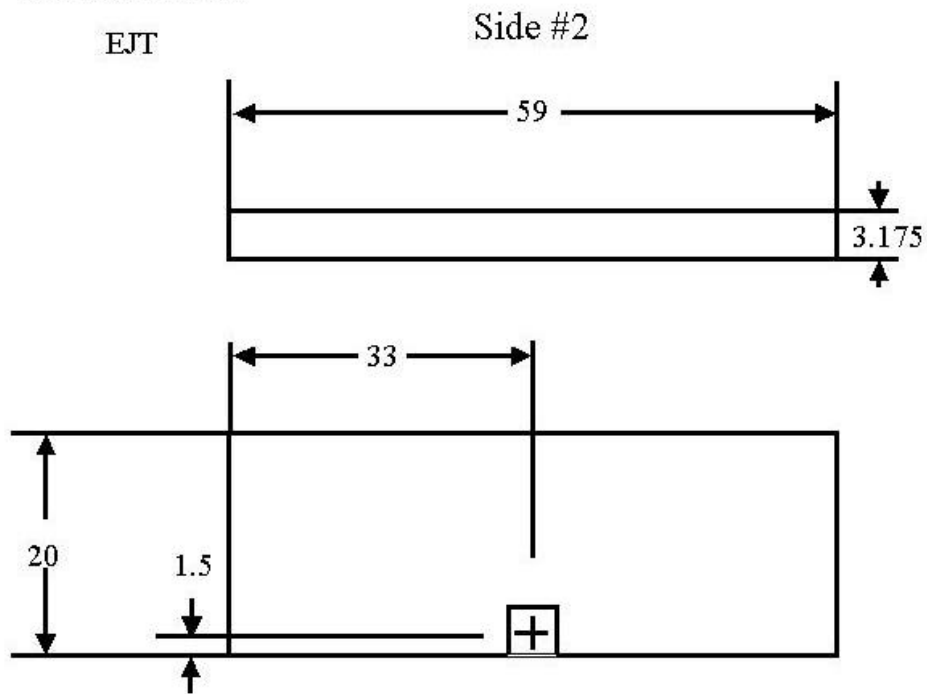


Figure B - 2. Side 2

Side 2 (made of plastic) is where the optical fiber enters the PLDS. Plastic is adequate since we have a low power laser. In order to use a high power laser anodized metal must be used. The PLDS has six walls altogether. The walls were glued together to form a box. However, the top of the PLDS was fixed to the PLDS by screws, so that it could be removed. The ability to remove the top allows the user to adjust the micro-optical components within. In general, the micro-optical components are fixed in place (with the exception of the translation plate).

Dimensions: mm

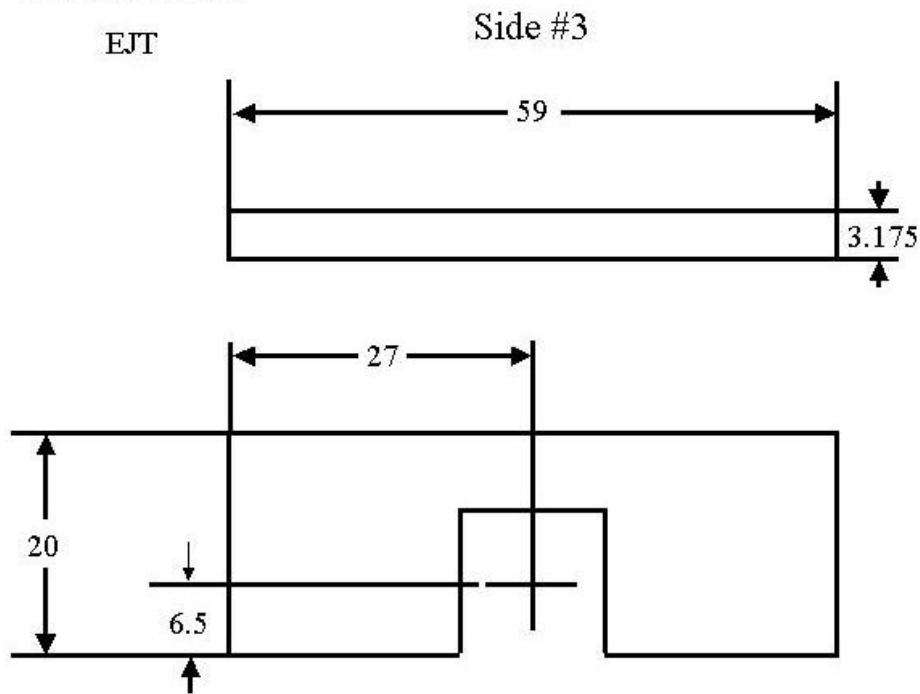


Figure B - 3. Side 3

Side 3 (made of plastic) is where the focus adjustment is made. Plastic is adequate since we have a low power laser. In order to use a high power laser anodized metal must be used. The PLDS has six walls altogether. The walls were glued together to form a box. However, the top of the PLDS was fixed to the PLDS by screws, so that it could be removed. The ability to remove the top allows the user to adjust the micro-optical components within. In general, the micro-optical components are fixed in place (with the exception of the translation plate).

Dimensions: mm

EJT

Side #4

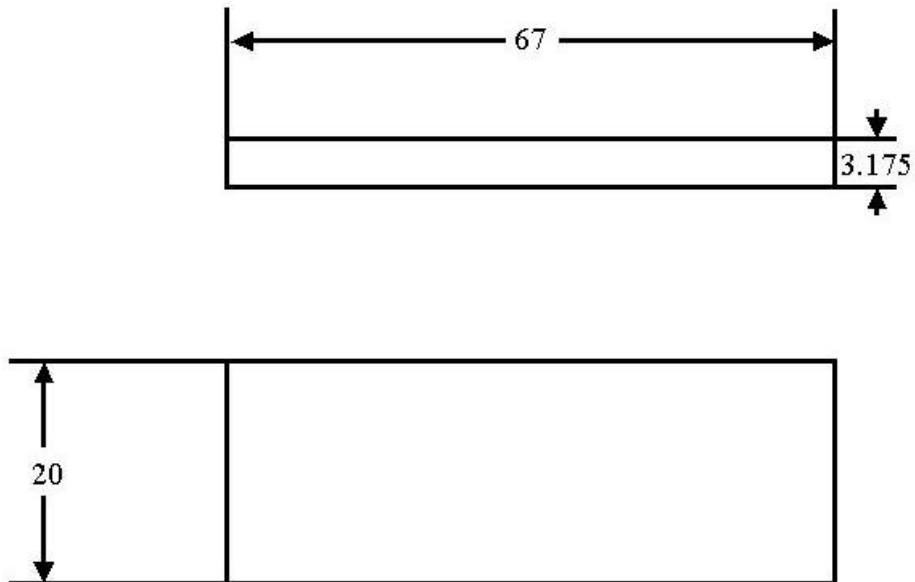


Figure B - 4. Side 4

Side 4 (made of plastic) is a complete wall with no holes in it. Plastic is adequate since we have a low power laser. In order to use a high power laser anodized metal must be used. The PLDS has six walls altogether. The walls were glued together to form a box. However, the top of the PLDS was fixed to the PLDS by screws, so that it could be removed. The ability to remove the top allows the user to adjust the micro-optical components within. In general, the micro-optical components are fixed in place (with the exception of the translation plate).

Dimensions: mm

EJT

Housing

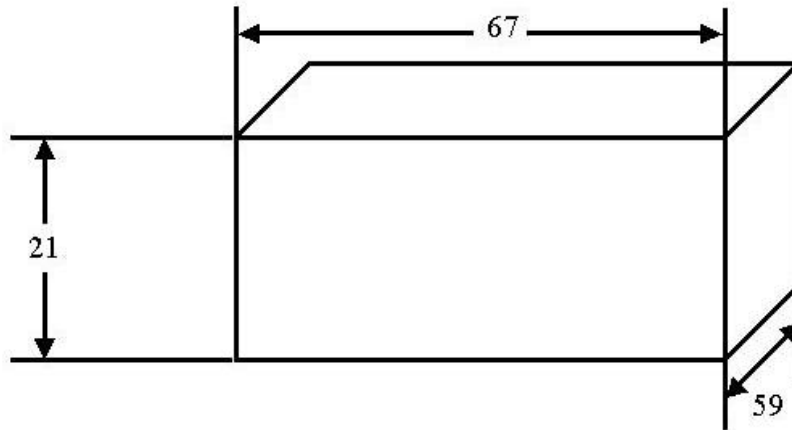


Figure B - 5. Housing

The plastic housing is adequate since we have a low power laser. In order to use a high power laser anodized metal must be used. The PLDS has six walls altogether. The walls were glued together to form a box. However, the top of the PLDS was fixed to the PLDS by screws, so that it could be removed. The ability to remove the top allows the user to adjust the micro-optical components within. In general, the micro-optical components are fixed in place (with the exception of the translation plate).

Dimensions: mm

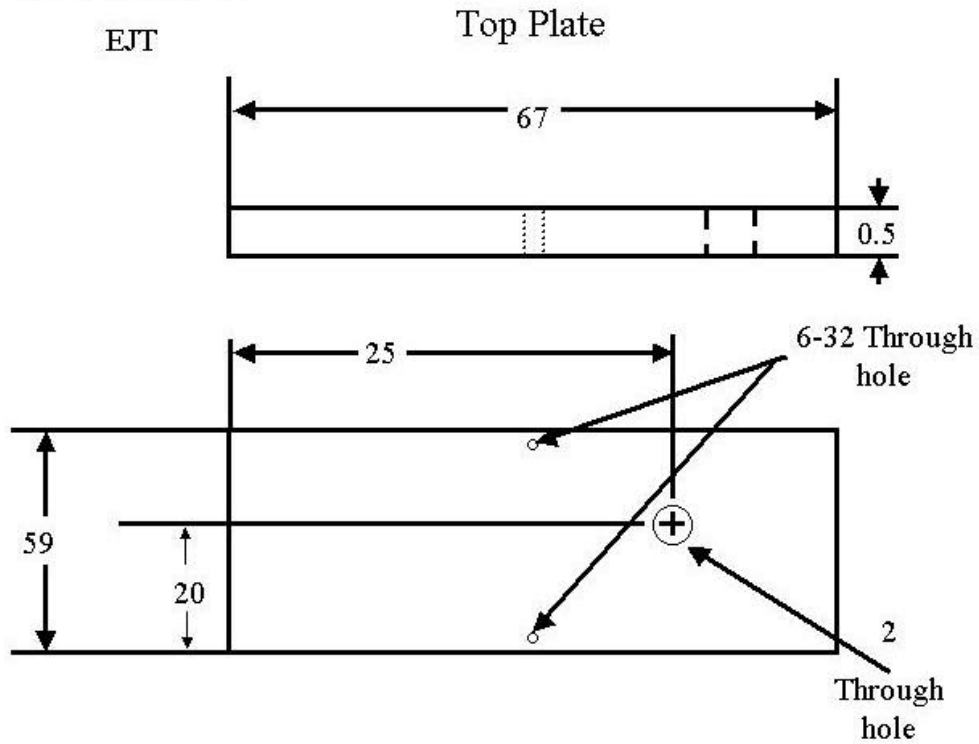


Figure B - 6. Top plate

The top plate (made of copper) is what supports the microscope slide. Copper had an additional benefit (by adding it at the top and the bottom of the PLDS), it made the PLDS more massive. The additional mass helps dampen low frequency ambient noise. The microscope slide was secured to the top plate by tape; this seemed to be sufficient friction to keep the microscope slide from moving with respect to the cantilever tip.

Dimensions: mm

EJT

Bottom Plate

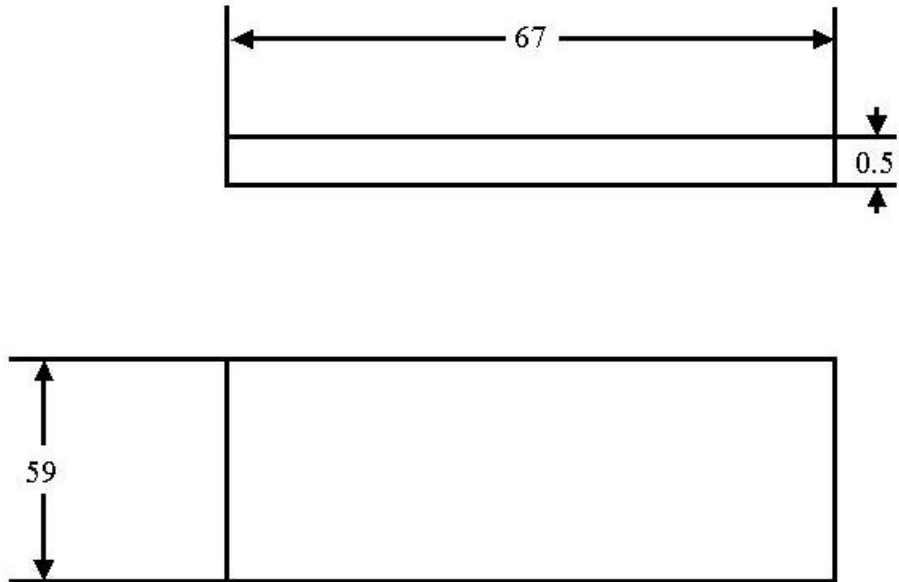


Figure B - 7. Bottom plate

The additional mass (of copper plate) helps dampen low frequency ambient noise. The microscope slide was secured to the top plate by tape, this seemed to be sufficient friction to keep the microscope slide from moving with respect to the cantilever tip.

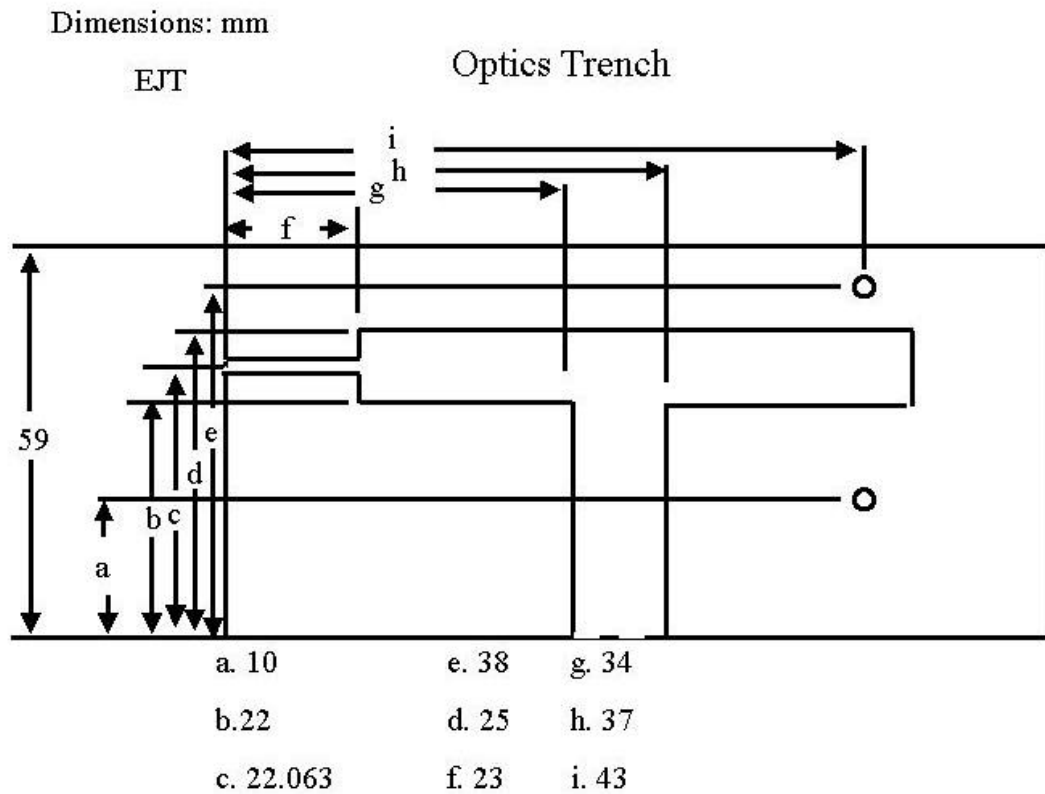


Figure B - 8. Optics trench

The optics trench (made of plastic) is milled to hold the fiber and the micro-optical components. Ideally it would be best to have the PLDS made to a tolerance of $\pm 100 \mu\text{m}$.

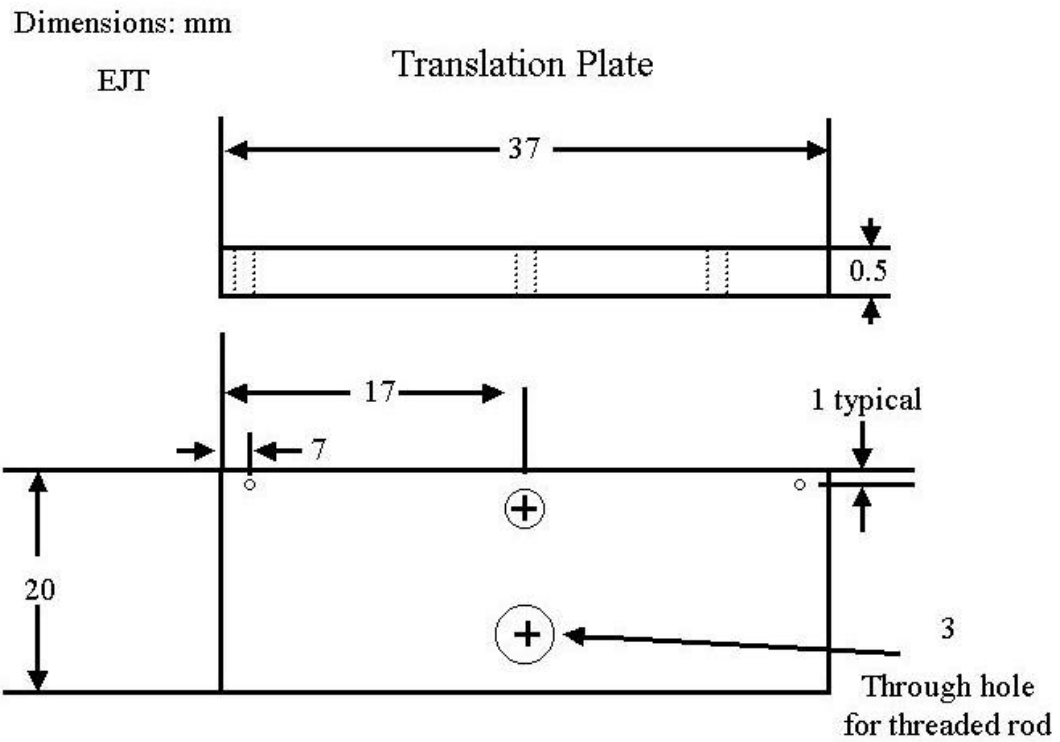


Figure B - 9. Translation plate

The translation plate (made of copper) holds the lens and the quarter-wave plate and is what moves when the focus is adjusted. This plate rests on top of a nut that is glued to a washer and copper tubing. The nut is on a threaded rod and by turning the washer the nut is translated up and down the threaded rod.

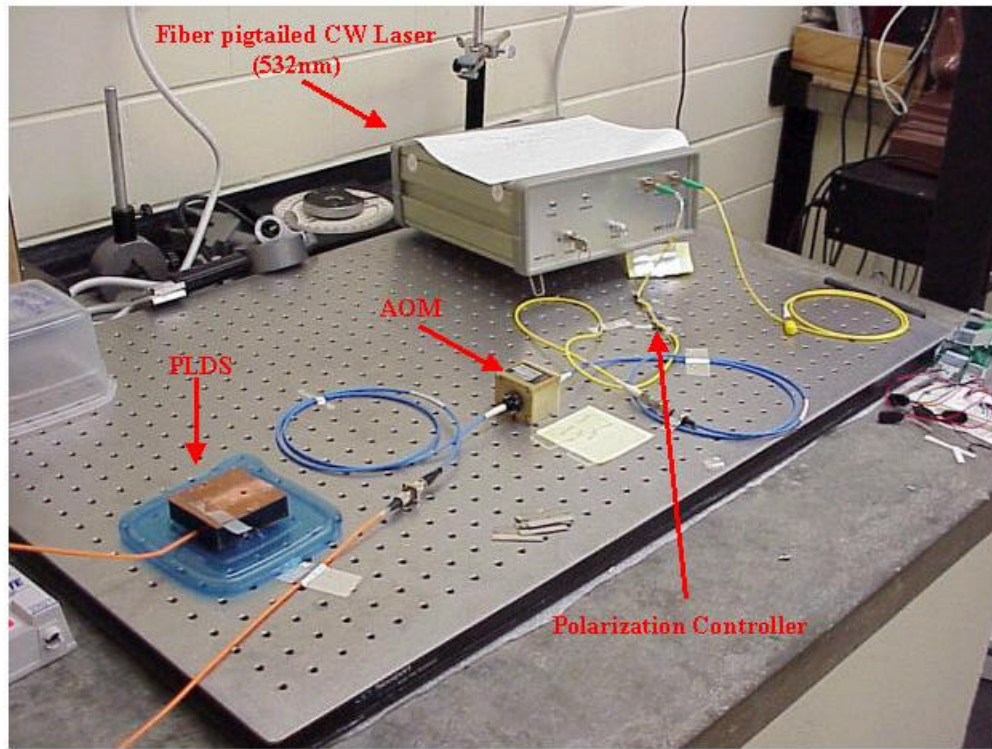


Figure B - 10. Experiment

The laser is fed into the AOM. The AOM is connected to a function generator when operating. The AOM allows light to pass when a square wave is high and does not allow light to pass when there is no voltage (the base of a square wave). The other side of the AOM is connected to the PLDS. The PLDS is small enough to fit onto the translation stage of the AFM.

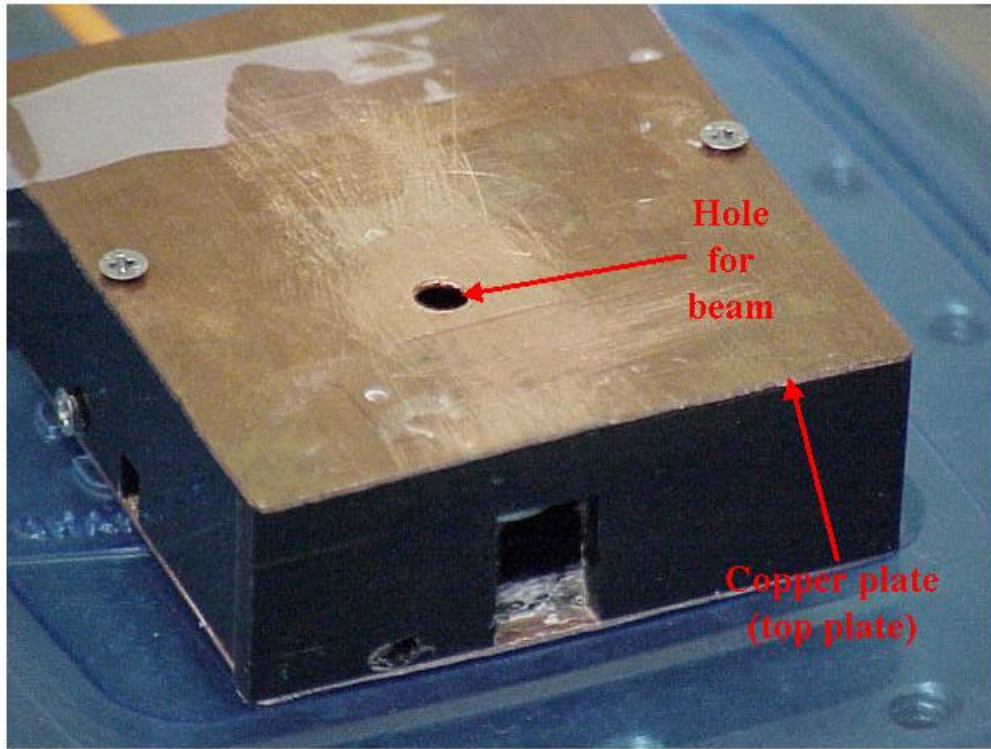


Figure B - 11. PLDS

The completed PLDS supports the microscope slide. The hole on the copper plate is where the laser beam exits the PLDS. The front rectangular hole (large) provides access to move the translation plate. The side rectangular hole (small) is where the photodetector can be placed.

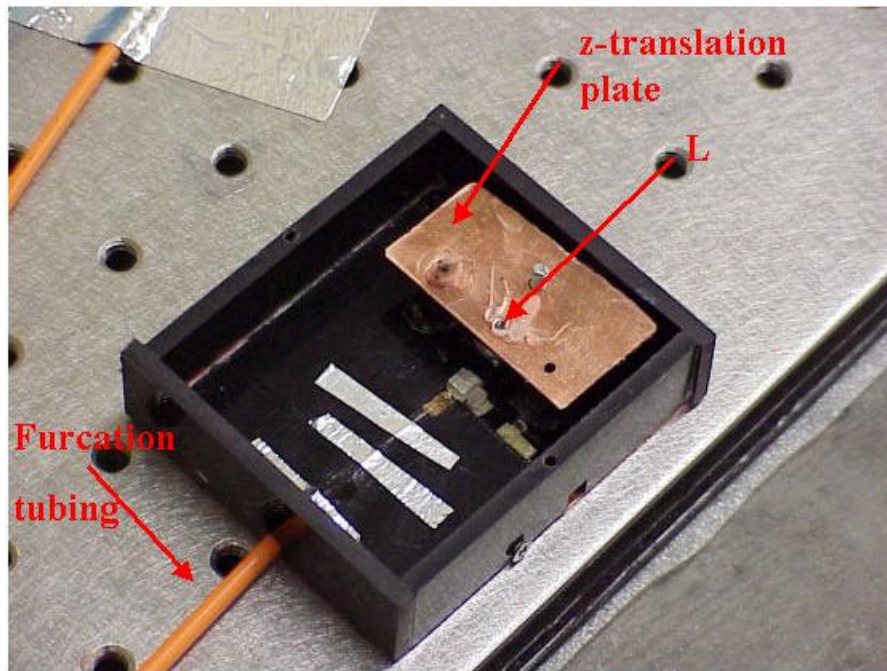


Figure B - 12. Inside the PLDS

The copper plate is the translation plate that supports the lens and quarter-wave plate. The optical components that are pointed out: fiber, furcation, and lens (L) for the translation plate (or the lens closest to the microscope slide).

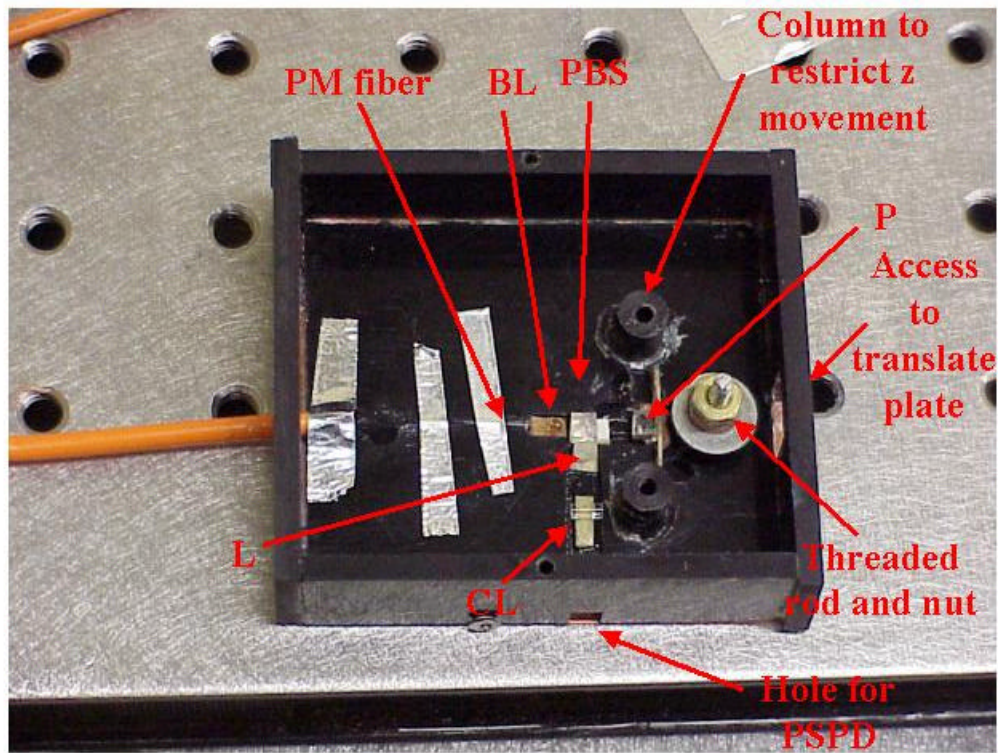


Figure B - 13. Inside the PLDS without translation plate

The translation plate has been removed so that the prism is visible. The brass nut is glued to a copper tubing, which is glued to a washer. Turning the washer causes the brass nut to move up and down the threaded rod. PM fiber = polarization maintaining single mode fiber, BL=ball lens, PBS=polarizing beam splitter, P=prism, L=lens, CL=cylindrical lens, PSPD=position-sensitive photodiode. The upper half of the micro-optical components is the first leg (PM fiber, BL, PBS, P, L). The lower half is the second leg (PBS, L, CL, PSPD).

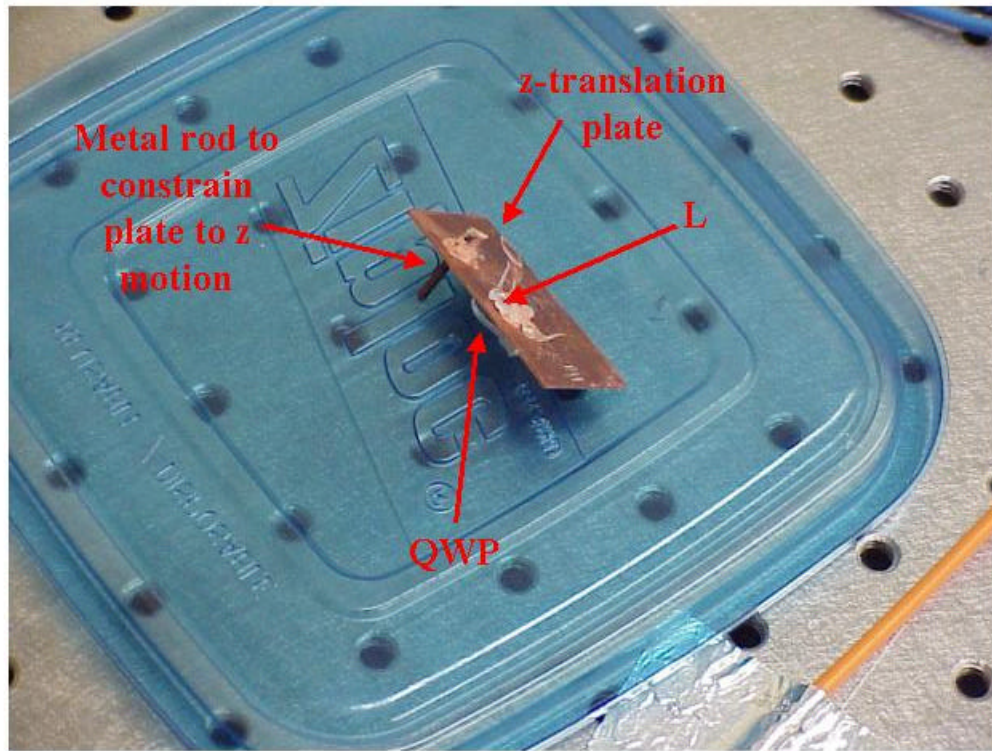


Figure B - 14. Translation plate

The leg is inserted into the plastic column, which (along with resting the back of the plate along the back wall of the PLDS) constrains motion of the plate to only the z direction.

QWP= quarter wave plate and L= lens. The lens on the translation plate is closest to the microscope slide.

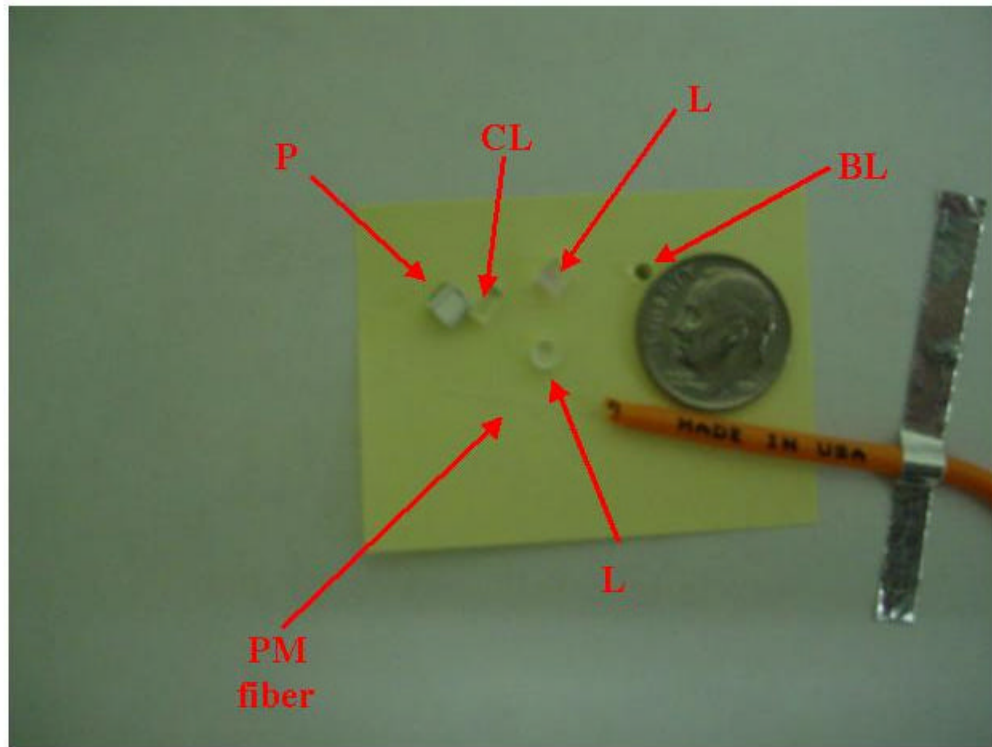


Figure B - 15. Optical components

Visible: prism (P), cylindrical lens (CL), ball lens (BL), lens (L) from the first leg (upper L), lens from the second leg (lower L), and the fiber (barely visible) with furcation (orange tubing).

Appendix

C. Design requirements

Before constructing an apparatus to deliver light to the tip-sample interface of an AFM, certain requirements must be met. The following will outline those necessities for each component of the experiment (further explanation of each component is found in the next section):

For the experiment:

I. Sample

- a. Must consist of photoactive molecules
 - i. WT-bR molecules are used.
- b. The photoactive molecules must:
 - i. Absorb light to initiate a conformational change
 1. WT-bR requires green, so we use a wavelength of 532 nm.
 - ii. The conformational change must be cyclic or reversible.
 1. WT-bR has a cyclic photocycle of about 5 ms.
 - iii. The conformational change must be measurable.
 1. WT-bR undergoes a height extension of 0.2 nm.
 - iv. The substrate used to hold the molecules must be transparent to green light.
 1. A glass microscope slide was used.
 - v. Light must be delivered from below the substrate.

1. The PLDS was designed to deliver light from below a microscope slide.

c. AFM

- i. Must be able to measure 0.2 nm deflection of the cantilever as a result of the photocycle of WT-bR.

1. The resolution of our AFM is 0.2 nm, so it is more likely to be able to measure the deflection of multiple layers.

- ii. Must have some room between the cantilever tip and the xy stage.

1. For our AFM the clearance was about 25 mm between the cantilever tip and the stage.

d. PLDS

- i. Must be able to place and remove from the AFM stage.

1. Therefore it must be:

- a. Less than 25 mm with the sample.
- b. Be fiber optically coupled, which makes the

PLDS easy to move.

- ii. Must be able to deliver:

1. Light that has pulse widths much less than 5 ms with a cycle time of 10ms.

2. The light must be green (we used 532 nm).

3. The spot size should be around 2 μm .

- iii. All the micro-optical components must fit within the PLDS.
 - 1. The design was supposed to mimic CD player optics.
 - iv. Must be able to deliver enough energy to initiate the photocycle.
- e. Laser
- i. Must be a green wavelength (we use 532nm).
 - ii. Must deliver:
 - 1. Light that has pulse widths much less than 5 ms with a cycle time of 10ms.
 - a. Our laser was a Nd:YAG frequency doubled continuous wave laser operating at 532 nm, so we used an AOM to chop the laser into pulses.
 - 2. Must be able to deliver enough energy to initiate the photocycle.
- f. AOM
- i. Must be able to chop the laser into pulse widths much less than 5 ms with a cycle time of 10 ms.
 - 1. Our AOM has a 70 nsec rise time and can be operated in pulsed or continuous mode.

- ii. Must be fiber optically coupled, so that it could be connected to both the laser and the PLDS.
- g. Fiber optics
 - i. Must use single mode polarization maintaining fiber.
 - 1. The numerical aperture should match among all the components.
 - 2. The type of fiber and connector must match among the various components.
 - ii. Must be able to connect the laser to the AOM, which is connected to the PLDS. Finally, the fiber must deliver the pulse of light to the micro-optical components within the PLDS.
 - 1. The cleave must be a good flat cleave.
- h. Micro-optical components
 - i. Must be able to propagate 532 nm wavelength.
 - ii. Design must be similar to the optics for CD players.
 - iii. They must be much larger in diameter than the optical fiber, so that the paraxial approximation is valid.
 - iv. The lens closest to the sample must be moveable, so that the focal point can be changed depending on sample thickness.
- i. The function generator
 - i. Must be able to run AOM.

- ii. Must be able to produce pulse widths much less than 5 ms with 10 ms intervals.
- j. Oscilloscope
 - i. Must be cable of digitizing collected data from the function generator and the AFM simultaneously.

Appendix

D. Challenges

Invariably for the design and construction of any experiment there are difficulties that arise. This appendix will point out a few of the largest difficulties encountered during the experimentation.

The main goal of the PLDS was to deliver pulses of light to photoactive molecules that were beneath a cantilever tip. The best way to do that was to require that the light be incident from below the sample, so that the molecules beneath the tip will be evenly illuminated. In order to accomplish that, the substrate for the photoactive molecules must be transparent to green light (the color that initiates the photocycle in WT-bR). Furthermore, the entire device must fit between the cantilever tip and the xy stage of the AFM.

Early during the design it was decided that purchase of “off the shelf components” and construction by hand would be the most efficient use of time and money. Balancing the requirements for the PLDS with what was readily available proved difficult. First, we had to invent a way for the light to be delivered to a sample from beneath. Immediately following, we decided that fiber optics would be best suited for the delivery of light to the sample. Although the idea to use fiber optics was very simple, the application was difficult. Because of the small distance between the cantilever tip and the xy stage (25mm), it was understood that just bringing the optical fiber close to the sample would not work within tolerance. If the optical fiber were brought close to the sample, the small distance (between sample and stage) could cause the fiber to bend too much (close to the critical bend radius) and, thus, possibly cause light to leak out at the bend (since the

requirement for total internal reflection would not be satisfied anymore). Furthermore, an optical fiber has a specific numerical aperture, which is a measure of how much the light diverges after exiting the fiber. Therefore, no matter the size of the core of fiber, a small spot size would not be achieved. The design to keep the optical fiber fixed horizontally initiated the introduction of the micro-optical components. If the fiber could be held horizontally, then the micro-optical components could condition and direct the light elsewhere in the small spaces that existed, which caused the optical design to be patterned after the optics of a CD player (since the optics are compact and can focus a spot to within in a 1mm distance). Finally, a rough idea of what the PLDS was to become was taking shape: a box with an optical fiber and micro-optical components with a hole in the top of the box to let the light out to a sample resting on top of the box.

Next, the purchase of a laser that had the required built in functions (small pulse widths at intervals of 10 ms with a 532 nm operating wavelength and plenty of power) within budget constraints was not possible. To combat this problem, we chose to purchase a continuous wave laser and an acoustical optical modulator (AOM). However, we needed to be able connect the laser, AOM, and PLDS in series, so that light would be delivered from the laser to the sample. This was solved easily by requiring all the components be fiber coupled (or pigtailed). By having the components coupled to optical fiber it would be trivial to connect all the components together (since they could all be connected in a similar fashion as to the way one connects BNC cables).

Connecting the components together through optical fiber was a great idea; however it was tougher to implement. To connect all the components together with very little power loss requires that all the components be built with the same type of optical

fiber. Construction of the AOM and PLDS resulted in the same optical fiber and connectors for both, which was single-mode polarization maintaining fiber (NA = 0.11) with FC/APC connectors. However, when the laser was built for us it was made with SMF-28™ fiber, which was not single-mode (at 532 nm; but it is single-mode for infrared wavelengths) or polarization maintaining. Furthermore, the connectors were FC/PC not FC/APC. This means there would be a mismatch in fiber type and connector type between the AOM and the laser, which would cause huge power losses. To try to minimize the power losses a jumper was bought (made of SMF-28™ fiber) that had an FC/PC connector on one side and an FC/APC connector on the other side. That solved the problem of connector type; however, there is still a mismatch in the fiber core size between the AOM and the laser. The problem could be totally solved by having the laser retrofitted with the correct optical fiber (that was not within budget).

With the idea for what a PLDS should be, in mind, more precise designs were formulated. However, there existed one more hurdle before the PLDS could be built. That problem was how to adjust the focal point of a lens into the sample space of photoactive molecules. One could imagine that some substrates are thicker than others; therefore, it would be convenient to be able to adjust (within 1 mm) the spot of the laser beam focus. As mentioned above the CD player design provided a base to work from. For the design of the CD player, they used a relatively complex system for feedback control to adjust the focus of a beam used to scan a CD. An electromagnetic coil system is wound on a translation plate (holding the focusing lens) such that when current is passed through the coil there is a Lorentz force that is induced, causing the translation plate to be pushed upward and downward (what type of current that was induced depended on what voltage

was measured from the PSPD). This system was not practical for our experiment. The design we invented was mechanical. A nut was attached to a washer (that had a larger diameter than the nut) and a spacer was placed between the nut and washer. The nut was then placed on a threaded rod fixed inside the PLDS. A slot was made in the side of the PLDS, which served as access to the washer. Turning the washer caused the nut to rotate and depending on which direction it rotated the washer and nut would move up and down the threaded rod. Then the translation plate need only rest on the nut, so that it too would move up and down the threaded rod. However, since the plate was held in place by only 2 points (the wall of the PLDS and the nut) the plate still could rotate slightly or tilt. To solve that problem a metal rod was added to the translation plate. The metal rod was placed in a shaft (the plastic column), which was free to move up and down in the shaft. Although the threaded rod and nut system was the best available, it is still not ideal. One still has try to access the hole for the washer while the cantilever is very close to the PLDS and even with tweezers this is a difficult task without moving the PLDS. However, currently the focusing mechanism (reflection of the laser off the cantilever, so that the PLDS-PSPD can be read) does not work, therefore translation of the plate is not important.

The next challenge arose when the micro-optical components were ready to be placed into the PLDS. The major issue is the alignment of the optics and their placement. The largest optical component had a diameter of 3 mm; it is important to understand the scale of the components because it illustrates just how small the PLDS was and the difficulty one might have in trying to align the micro-optical components within the PLDS by hand. The diameter of the optical fiber was 125 μm and this too was aligned by

hand. Ideally the optical fiber axis should be perfectly aligned with the optical axis of the PLDS. However, perfect alignment by hand was not possible. One could imagine that an equally difficult task of trying to align a single strand of hair along the optical axis (since a single strand of hair and the optical fiber are of the same size). In addition to the alignment along the optical axis, the fiber was to have the correct orientation with respect to the polarizing beam splitter. The fast and slow axis of the fiber must be aligned with the polarizing beam splitter such that only the transverse electric mode is transmitted through the beam splitter. Any slight misalignment in the angular rotation of the optical fiber with respect to the beam splitter would cause some power loss. Maximizing the power through the beam splitter minimized the problem (the output from the end of the optical fiber was about 2 mW and the power through the beam splitter was about 1.5 mW).

One last additional challenge worth mentioning was related to the optical fiber cleave. Power output can be very dependant on the cleave of the end of a fiber. Proper mechanical devices exist that will make very nice flat cleaved fiber; however, these machines are very expensive, so they are reasonable choices when one will be making many fiber cleaves. The PLDS only required a single fiber cleave, so purchase of a fiber cleaver was not practical. Therefore, the fiber cleave was performed manually (the same concept was employed to cleave the fiber that a fiber cleaver uses). The method was to strip the bare fiber of the outer coating, score the glass fiber (creates a stress fracture), and then place the end of the fiber under tension. If the score is straight and the tension is the right amount, the fiber will cleave with a perfect flat end. However, in reality (when cleaving by hand), the score nor the tension is perfect, which leads to a fiber end face that

is not flat. To minimize the problem, the shape of the beam from the end face was observed (the more Gaussian it looked the better the cleave) and the power output was measured (the greater the power the better the cleave).

Appendix

E. Bibliography

- ¹ C. Huang, C. Wang, D. S. Mehta, and A. Chiou, *Optics Communications* **195**, 41-48 (2001).
- ² R. R. Birge, N. B. Gillespie, E. W. Izaguirre, A. Kusnetzow, A. F. Lawrence, D. Singh, Q. W. Song, E. Schmidt, J. A. Stuart, S. Seetharaman, and K. J. Wise, *J. Phys. Chem. B*, **103**, 10746-10766 (1999).
- ³ T. Hugel, N. B. Holland, A. Cattani, L. Moroder, M. Seitz, and H. E. Gaub, *Science* **296**, 1103-1106 (2002).
- ⁴ C. H. Foyer, in *Photosynthesis*, (John Wiley & Sons, Inc., New York, 1984), Vol. **1**.
- ⁵ B. B. Buchanan, W. Gruissem, and R. L. Jones, in *Biochemistry and molecular biology of plants*, (American society of plant physiologists, rockville, 2000).
- ⁶ S. M. Danks, E. H. Evans, and P. A. Whittaker, in *Photosynthetic Systems*, (John Wiley & Sons, Inc., New York, 1983), Chap. 2, p.65.
- ⁷ M. Webster, in *Merriam Webster's Collegiate Dictionary*, **10th** edition, (Merriam-Webster, Incorporated, Springfield, 1997).
- ⁸ G. Binning, C. F. Quate, and Ch. Gerber, *Phys. Rev. Lettr.* **56**, 930-933 (1986).
- ⁹ I. Rousso, E. Khatchatryan, I. Brodsky, R. Nachustai, M. Ottolenghi, M. Sheeves, and A. Lewis, *J. Structural Biology* **119**, 158-164 (1997).
- ¹⁰ N. Periske, M. Pfeiffer, R. Guckenberger, and M. Fritz, *Colloids and Surfaces B: Biointerfaces* **19**, 325-332 (2000).

- ¹¹ Peter K. Cheo, in *Fiber optics devices and systems*, edited by G. K. Chenenko (Prentice-Hall, Inc., Englewood Cliffs, 1985), Chap. 6, p.88-117.
- ¹² Hiroshi Maturata, *Handbook of optical fibers and cables* (Marcel Dekker, Inc., New York, 1988), Chap. 2, p.15-178.
- ¹³ L. B. Jeunhomme, in *Sungle-mode fiber optics principles and applications*, edited by B. J. Thomson (Marcel Dekker, Inc., New York, 1983), Chap. 6, p.178-180.
- ¹⁴ P. K. Cheo, in *Fiber Optics Devcies and Systems*, edited by N. Holonyak, Jr. (Prentice-Hall, Inc., Englewood, 1985), Chap. 6, p.113-117.
- ¹⁵ H. Murata, in *Handbook of optical fibers and cables*, edited by B. J. Thomson (Marcel Dekker, Inc., New York, 1988), Chap. 4, p.312-374.
- ¹⁶ R. R. Shannon, in *The art and science of optical design*, (Cambridge University Press, Cambridge, 1997).
- ¹⁷ D. C. O'Shea, in *Elements of modern optical design*, (John Wiley & Sons, Inc., New York, 1985).
- ¹⁸ A. Walther, in *The ray and wave theory of lenses*, edited by P. L. Knight (Cambridge University Press, Cambridge, 1995).
- ¹⁹ S. Timshenko, *J. Opt. Soc. Am.* **11**, 233 (1925).
- ²⁰ O. Marti, A. Ruf, M. Hipp, H. Bielefeldt, J. Colchero, and J. Mlynek, *Ultramicroscopy* **42-44**, 345 (1992).
- ²¹ M. Allegrini, C. Ascoli, P. Baschieri, F. Dinelli, A. Lio, and T. Mariani, *Ultramicroscopy* **42-44**, 371 (1992).

- ²² R. G. Stearns and G. S. Kino, *Appl. Phys. Lett.* **47**, 1048-1050 (1985).
- ²³ J. R. Barnes, R J. Stephenson, C. N. Woodburn, S. J. O'Shea, M. E. Welland, T. Rayment, J. K. Gimezewski, and Ch. Gerber, *Rev. Sci. Instrum.* **65**, 3793-3798 (1994).
- ²⁴ P. G. Datskos, S. Rajic, and I. Datskou, *Appl. Phys. Lett.* **73**, 2319-2321 (1998).
- ²⁵ P. G. Datskos, M. J. Sepniak, C. A. Tipple, and N. Lavrik, *Sensors and Actuators B* **76**, 393-402 (2001).
- ²⁶ P. G. Datskos, S. Rajic, M. J. Sepaniak, N. Lavrik, C. A. Tipple, L. R. Senesac, and I. Datskou, *J. Vac. Sci. Technol. B* **19**, 1173-1179 (2001).
- ²⁷ A. Subramanian, P. I. Oden, S. J. Kennel, K. B. Jacobson, R. J. Warmack, T. Thundat, and M. J. Doktycz, *Appl. Phys. Lett.* **81**, 385-387 (2002).
- ²⁸ D. Halliday, R. Resnick, and J. Walker, in *Fundamentals of physics*, 4th edition, edited by C. Mills (John Wiley & Sons, Inc., New York, 1993), Chap. 19, p.540-541.
- ²⁹ R. J. Roark and W C. Young, in *Formulas for stress and strain*, 5th edition, edited by T. G. Hicks (McGraw-Hill, New York, 1975), Chap. 7, p.91.
- ³⁰ S. Timoskenko, *J. Opt. Soc. Am. & Rev. Sci. Instr.* **11**, 233 (1925).
- ³¹ H. Sasabe, T. Furuno, A. Sato, and K.M. Ulmer, *Proceedings of the Annual International Conference of the IEEE Engineering in Medicine and Biology Society* , 1003, (1988).
- ³² J K. Lanyi, *Biochemistry*, **66**, 1192-1196 (2001).

- ³³ J. Fitter, M. Adams, G. Coddens, G. Buldt, A. Dencher, and R.E. Lechner, *Physica B* **213-214**, 775-779 (1995).
- ³⁴ K.A. Fisher, S.L. Whitfield, R.E. Thomson, K.C. Yanagimoto, M.J. Gustafsson, and J. Clarke, *Biochimica et Biophysica Acta*, **1023**, 325-334 (1990).
- ³⁵ N. Persike, M. Pfeiffer, R. Guckenberger, and M. Fritz, *Colloids and Surfaces B: Biointerfaces*, **19**, 325-332 (2000).
- ³⁶ N. Hampp, *Chem. Rev.* **100**, 1755-1776 (2000).
- ³⁷ H. Kuhn and C. Kuhn, *Chem. Phys. Lettr.* **253**, 61-68 (1996).
- ³⁸ Q. W. Song, X. Wang, R. R. Birge, J. D. Downie, D. Timucin, and C. Gary, *J. Opt. Soc. Am. B* **15**, 1602-1609 (1998).
- ³⁹ D. J. Muller, C. Schoenenberger, F. Schabert, and A. Engel, *J. Structural Biology* **119**, 149-157 (1997).
- ⁴⁰ *Oxford dictionary of physics*, **4th** edition, edited by A. Isaacs (Oxford University Press, Oxford, 2000), p.19.
- ⁴¹ *McGraw-Hill Encyclopedia of physics*, **2nd** edition, edited by S. P. Parker (McGraw-Hill, New York, 1991), p.5-6.
- ⁴² J. A. Cope, *Phys. Educ.* **28**, 15 (1993).
- ⁴³ J. He, L. Samuelson, L. Li, J. Kumar, and S. K. Tripathy, *Langmuir* **14**, 1674-1679 (1998).
- ⁴⁴ R. R. Birge, *Annu. Rev. Phys. Chem.* **41**, 683 (1990).